Experimental static and dynamic response of RC beams damaged and strengthened with NSM GFRP rod

Experimental static and dynamic response of RC beams damaged and strengthened with NSM GFRP rod

R. Capozucca[1], E. Magagnini[2] and M.V. Vecchietti[3]

Abstract

Inserting FRP rods into grooves using the NSM technique has been demonstrated to be a suitable method for repairing reinforced concrete (RC) beams. There is limited experience with the use of GFRP in the strengthening of RC elements due to low Young's modulus of glass fibers. The aim of the paper is to analyse the static and dynamic behaviour of RC beams damaged and strengthened by glass fiber reinforced polymer (GFRP) rods utilizing the near surface method (NSM). Undamaged and damaged three RC beams have been experimentally tested under bending loading with and without strengthening by GFRP rods. For a beam, damage has been represented firstly by notches on concrete cover. The beam has been successively strengthened by epoxy resin and NSM GFRP rod and then subjected to bending tests. Vibration tests have been adopted as nondestructive method of control during the experiments to assess the response of RC beams at different damage steps of concrete or due to decrease of bond of GFRP rod. Vibration tests foresaw two boundary conditions, respectively, free-free and hinged ends. Experimental static and vibration results are below shown; discussion and comments on the strengthening bond of NSM GFRP rod have been developed.

Keywords: RC beams; damage; GFRP rod; NSM of strengthening; vibration tests; bond.

1. Introduction

[1]Professor of Civil Structural Engineering, DICEA, University Politecnica delle Marche, 60100 Ancona, Italy. Ph. +39.071.2204570 Fax +39.071.2204532 r.capozucca@staff.univpm.it
[2]PhD Eng., DICEA, University Politecnica delle Marche, 60100 Ancona, Italy.
[3]PhD student, DICEA, University Politecnica delle Marche, 60100 Ancona, Italy.

The strengthening of damaged reinforced concrete (RC) structures is a relevant topic of civil engineering and the use of fiber-reinforced composites has been increased in recent years. Unfortunately, not all the aspects related to the behaviour of composite materials in the structural strengthening of RC elements have been completely solved, although many experimental and theoretical studies have been developed. The technique that involves the use of fiber-reinforced polymers (FRPs) as plates and/or sheets glued onto concrete surface is one of two principals' methods adopted to strengthen RC structures. This technique has been applied just many years ago [1,2] in Switzerland and Germany. More recently, the investigations [3-6] and analytical models [7-10] for predicting the influence of different parameters were also proposed. Another one technique to strengthen RC elements is to use FRP rods inserted into grooves on concrete covers; this technique is named near surface method (NSM). NSM as strengthening of RC beams appears capable to solve many aspects such as full FRP tension strength and to avoid damage deriving from impact and high temperature. This type of strengthening has been investigated by experimental tests and theoretical analysis [11-14] also analysing the different factors affecting the bond of NSM FRP bars in concrete [15-16]. Although composite materials, similar to isotropic materials, can be subjected to various damages: cracks in fiber, in matrix and in interfaces of fibers and matrix, experimental tests have been demonstrated the availability of NSM FRP technique also in presence of local damages of composite rods [17]. The knowledge of static behaviour of RC beams strengthened with the NSM technique in the last decade has grown based on experimental and theoretical researches; however, between the FRPs the use of GFRP rods in the strengthening of RC beams is still an open field of research [18-22]. GFRP composite material is characterized by low Young's modulus and not relevant value of strength although the ultimate elastic strain under tensile stress is sufficiently adequate in the practice. Composite material GFRP rods with its mechanic characteristics in strength-

ening by the NSM technique calls for additional in-depth analysis. The availability of NSM GFRP strengthening in RC beams is based on at least two important factors: the maintaining of bond between NSM rods and concrete and/or adhesive resin until failure of beam; the capacity of GFRP rods to increase strain under tension until the failure by compression of concrete which is the conventional ultimate condition for RC beams under bending.

In this paper, all enounced problems have been experimental analysed considering the static response of three RC beams tested under bending loading with and without NSM GFRP rod strengthening. The vibration response of RC beams has been adopted as additional non-destructive method to control the damage condition of beams [23-25]. Vibration frequency data have been acquired by experimental dynamic tests assuming as boundary conditions free ends and hinged ends; the dynamic tests were carried out on RC beams with and without strengthening, at different steps of damage degrees obtained by static bending tests or by notches. One RC beam has been studied with damage due to notches on extrados concrete cover of beam and strengthened by epoxy resin inside the notches and NSM GFRP rod at intrados concrete cover. After strengthening, the beam has been subjected again to the same loading path. The analysis of free vibration of beams as non-destructive method has been carried out to assess RC beams strengthened with and without NSM FRP rods. There are several scientific reports in literature regarding the use of vibration data for damage identification in controlled conditions or in numerical simulations of elements having mainly homogeneous material [26-31]. The basic concept behind vibration monitoring is that dynamic characteristics are functions of structures' physical properties, therefore any change caused by damage results in change in dynamic response. Further, two tested RC beams were affected by different damages due to increasing cracking of concrete for bending tests and one beam by artificial damage due to notches on compressive side. In the

NSM strengthening bond-slip may be influenced by the cracking of concrete and loss of adhesion of rods which can modify frequency values and beams' modes of vibration.

Below, experimental static and dynamic tests are described; results obtained in terms of static response and frequency values are shown and discussed. Finally, an analysis of bond of strengthened RC beams based on experimental data allows obtaining useful coefficients to estimate the reduction of strain of GFRP rod compared to the Bernoulli's hypothesis of bending plane.

2. Static response of RC beams damaged and strengthened by NSM GFRP rod

Three RC beams, named B1-B2-B3, were built with materials of following mechanical parameters: concrete of strength $f_c \cong 40.00$ N/mm² and Young's modulus $E_c \cong 34.5$ kN/mm²; steel reinforcement with yield strength $f_y \cong 500$ N/mm² and Young's modulus $E_s = 210$ kN/mm². Four longitudinal steel bars of diameter 10mm and stirrups of diameter 6mm were used. In Figure 1(a) the specimen of RC beam of length 2.20m and rectangular section 120mm·160mm is shown with presence of one groove at intrados of section 20mm·20mm where, after static tests without strengthening, the GFRP rod has been inserted and glued. In Figure 1(b) set up of simply supported RC beam for static bending tests is shown.

The GFRP rods used on are of Company *MAPEI*. The mechanical and geometrical parameters of the GFRP rods were experimentally derived by tensile tests carried out on 2 specimens (Tab. 1); failure of specimens was of the XGM type - *Explosive, Gage, Middle* – as indicated in ASTM D-3039 Standard [32]. The adhesive used to glue reinforcement of GFRP rod was a two-component epoxy structural adhesive with high capacity to adhere to concrete surfaces. Three specimens of 40mm·40mm·160mm size were tested and subjected to compression tests to determine the mechanical characteristics of adhesive (Fig. 2). Each

specimen was instrumented with two strain gauges to determine the vertical and horizontal strains; the values of Young's modulus and Poisson's coefficient determined are, respectively, E_{adh} =1597N/mm^2 and v_{adh} ≈0.48.

2.1. Bending test on beam B1

The RC beam B1 was the first beam subjected to bending test, according to the set-up of simply supported beam with hinge restraints (Fig. 1(b)). The instrumentation used was as following: one vertical jack and one load cell to evaluate vertical load value during bending test; three LVDTs to measure deflections at midspan and close to restraints; LVDTs to record strains at midspan of beams at the top and bottom on midspan section (Fig. 3).

Main results obtained during the static bending test are summarized in Table 2 where damage degree is shown as *Di* with *i*=1,2,3 and it's linked to the value of bending load *Pi* reached at each one of the three cycle of bending loading.

The choice of these load cycles has permitted to damage beam B1 with cracks on concrete reaching the maximum experimental value of steel strain equal to $\varepsilon_s \cong 3.35 \cdot 10^{-3}$ for damage degree D3, higher than yield strain value of steel. From the measurements recorded in terms of deflection and strains at midspan of beam B1, the experimental diagrams shown in Figures 4 have been obtained. From these data it is possible to characterize the response of beam B1 before the strengthening with NSM GFRP rod. The experimental moment, *M*, versus curvature, χ, diagram obtained at each cycle of loading for the cross section at the beams' mid length is shown in Figure 5. The maintaining of plane section of RC beam is underlined by the measurement of strains obtained at midspan of beam for edge compressive concrete and at the level of steel bars (Fig. 6). Finally, in Figure 7 the cracking damages of RC beam at each load cycle, *Di* with *i*=1,…, 3, are shown.

After *D3* damage degree, the B1 beam was strengthened with GFRP circular rod inserted in the groove by adhesive epoxy resin and subjected to a similar loading path for the load step *D1*, *D2* and *D3* and, subsequently, subjected to a load equal to *P*=28kN for an added damage degree *D4*. Table 3 shows the values acquired from the instrumentation used for each loading step and the curvature at the midspan section.

Figure 8 shows experimental diagram load, P, versus deflection, δ, at midspan section of beam and diagram load, P, versus strain, ε_{GFRP}, of GFRP rod. The experimental diagram moment, M, versus curvature, χ, evaluated considering the strains on compressed edge of midspan section and on GFRP rod, is shown in Figure 9.

The distribution of the experimental strain values recorded at damage degree *Di* at the mid span section is represented in Figure 10 considering the points of compressive edge of concrete, tensile steel and tensile GFRP rod. In this case the section's real behaviour is not plane because the strains on the GFRP rod aren't linearly congruent with the strains of steel and of the compressed concrete fiber and are conditioned by a *stress-strain lag*.

Finally, Figure 11 shows the crack pattern that occurs in the strengthened beam at the damage degree *D4* at the failure of beam.

2.2 Bending test on beam B2

The beam B2, similar to beam B1 for the material used, was strengthened using a GFRP rod and it was artificially damaged on the concrete cover in the central extrados area with 5 notches of section equal to 20·20mm with development normal to the axis of the beam. The different artificial notching damage steps are the following: damage *D1** with one notch at the midspan; *D2** with three notches, interaxle spacing 150 mm; *D3** with five notches, interaxle spacing 150mm. Notches were subsequently filled with epoxy resin (Fig. 12(a)) and static cyclic bending tests were performed. Instruments adopted during the tests

allowed measuring deflection, strain, and vertical load. Three strain gauges were located on the compressive extrados surface, respectively two on concrete and one on resin, to measure compressive strain (Fig. 12(b)); one strain gauge was placed on the steel rod at the beam's mid span to measure tensile strain. The beam's deflection was measured experimental using vertical LVDTs.

The strengthened RC beam B2 with notches filled by resin has been subjected to bending tests foreseeing four loading cycles with vertical loads equal to P = 4 kN, 8 kN, 16 kN and 28 kN, and, successively, the ultimate loading test until failure. Each load step corresponds to a configuration of the static damage already identified for the strengthened beam B1: *D1*, *D2*, *D3* and *D4*. The failure of beam B2 was reached at load values equal to P≈37.35kN. The main experimental data obtained by bending tests are shown in Table 4. In Figure 13, experimental diagram load, P, versus deflection δ, at midspan section of beam and diagram load, P, versus strain at the edge of compression concrete, ε_c, are shown. In Figure 14, the strain values measured on the resin inserted on notch, ε_{res}, are shown for the all damage degrees. It is noted that the maximum value of strain in the resin inserted in the notch reached high value of deformation equal to about $7\cdot 10^{-3}$. In Figure 15 the diagram of the moment, M, versus curvature, χ, relative to the cross-sectional area, is shown with reference to the values measured by LVTDs applied on the compressive concrete and on steel bar.

The cracking caused by load level P=8.0kN (*D2*) and P=16.0kN (*D3*), is shown in Figure 16.

After applying the last load cycle, P = 28.0 kN, the beam was subjected to an increasing load until the ultimate load that was equal to P= 37.0 kN.

The failure occurs by the crash at the extrados of compression concrete cover containing the notches filled with resin (Fig. 17).

2.3. Bending test on beam B3

The RC beam B3 has been subjected to the same loading path of beam B1 with three loading and unloading cycles: *D1*=4kN, *D2*=8kN, *D3*=18kN utilizing the same apparatus and instruments. The main experimental results acquired for each loading-unloading step and an elaboration of the data to obtain the curvature of the mid-section are shown in Table 5. The experimental diagram load, P, versus deflection, δ, for beam B3 under bending tests is represented in Figure 18. The cracking damage development due to bending test at different damage degrees *Di*, i=1,2,3 for RC beam B3 without strengthening is shown in Figure 19.

The damaged beam B3 was strengthened with NSM GFRP rod and subjected to the same three loading-unloading cycles. Successively, the beam was subjected to increasing load till failure. Main experimental results obtained from bending test are shown in Table 6.

In Figures 20(a), (b) and (c) the experimental diagrams load, P, versus deflection, δ; strain on compressive concrete, ε_c, and tensile steel, ε_s, for the strengthened beam B3 are shown. The distribution of the experimental recorded strains by bending test for the mid span sections of the strengthened beam B3 is represented in Figure 21, where the development of curve is not linear.

The collapse, reached at a load value equal to P=33 kN (Fig. 22), happened with crushing of the compressed concrete and successively expulsion of the concrete cover at the intrados with detachment of the GFRP rod.

3. Vibration response of beams

As a first approximation, an undamaged RC beam model may be assumed as a uniform slender beam. For a beam in flexure only the component of displacement $v(x,t)$ may be consider neglecting gravity forces, the effects of rotary inertia, shear deformation and damping. The inertia force of the element is $\rho A \frac{\partial^2 v}{\partial t^2}$ with ρ is density of the material and A is the cross-sectional area. In the case of natural vibration of a beam of homogeneous material, the well-known equation is obtained following the Euler-Bernoulli's theory:

$$\frac{\partial^2}{\partial x^2}\left(EI\frac{\partial^2 v}{\partial x^2}\right) + \rho A \frac{\partial^2 v}{\partial t^2} = 0 \quad (1)$$

where: E is Young's modulus; I is the second moment of area of the cross-section; ρA is the mass per unit length of beam. The solution of Eq. (1) is given in the following form:

$$v(x,t) = V(x)\,cos(\omega t - \alpha) \quad (2)$$

where ω is the circular frequency and α is a phase angle. Introducing Eq. (2) in Eq. (1), the following is obtained:

$$\frac{\partial^2}{\partial x^2}\left(EI\frac{\partial^2 v}{\partial x^2}\right) + \rho A \omega^2 V = 0 \quad (3)$$

Eq. (3) is simplified in the following way:

$$\frac{d^4 V}{dx^4} - \lambda^4 V = 0 \quad (4)$$

with $\lambda^4 = \frac{\rho A}{EI}\omega^2$. The general solution is shown below:

$$V(x) = B_1\,sin\,\lambda x + B_2\,cos\,\lambda x + B_3\,sin\,\lambda x + B_4\,cos\,\lambda x \quad (5)$$

Eq. (5) defines the natural dynamic behaviour of a beam without any consideration on the constraints at the ends. Five unknown parameters need to be determined: the constants B_i per $i=1,2,3,4$ and the eigenvalue λ. The problem may be solved considering the equilibrium and compatibility equations for the boundary conditions [33]. The expression of circular natural frequency ω_r^f for generic mode r of vibration, in the case of *both ends free*, is

obtained:

$$\omega_r^f = \left(a_r \frac{r\ \pi}{L}\right)^2 \sqrt{\frac{EI}{\rho A}} \tag{6}$$

being the eigenvalue $\lambda_r = r\frac{\pi}{L}$ for a simply supported beam. The eigenvalue for a free end beam at the *r* mode λ_r^f may be correlated to the value λ_r for a simply supported beam:

$\lambda_r^f = a_r \cdot \lambda_r$ with a_r = coefficient that depends on the different *r* mode of vibration, equal to 1.506, 1.25, 1.167, 1.125 respectively, for the first four modes.

Table 7 contains the parameters relative to tested beams for the theoretical evaluation of the frequencies obtained with Eq. (6) for the undamaged beam D0.

In the Table 8 the frequency values of undamaged experimental beams B1 and B3 following the Euler-Bernoulli (EB) model are shown.

The experimental dynamic test was carried out at first on a RC beam undamaged using the common technique where a mobile accelerometer measures the acceleration of the structural element triggered using a specific impact hammer (*Brüel & Kjær, Type 8202*) in a fixed point (Fig. 23). The accelerometer used in the dynamic experiment was a *Brüel & Kjær* produced *Piezoelectric CCLD brand no 4508.* The dynamic test, on all the specimens, was carried out recording the response of the structure in nine positions, $Mark_i$ with *i*=1,…9, to trigger with an impact hammer in a fixed position; recorded frequency values are the average of 10 beats for every location of accelerometer. A Fast Fourier Transformation two-channel analyzer, *Multichannel Data Acquisition Unit 2816 Type,* and PULSE Lab shop software were used for data acquisition (Fig. 23(a)).

Experimental vibration tests were carried out considering two constraints conditions: free-free ends and hinges at the ends. In the case of free ends an elastic spring has been adopted to simulate this condition (Fig. 23(b)) and in the case of hinged ends the beam was located on metal hinge devise.

The theoretical and experimental frequency values obtained for undamaged beams B1and B3 are shown and compared in Table 8. In Figure 24, the first four modal shapes experimentally obtained for B3 beam model have been reported.

* * *

The beam B1 subjected to bending tests and therefore damaged by cracking of concrete by bending was subjected to free vibration in the condition of hinge-hinge constraint. The main experimental frequency values data obtained from the analysis of free vibration for RC beam B1, without and with GFRP NSM strengthening, at the various damage steps *Di*, are contained in the Tables 9 and 10. Average frequency values were recorded experimentally at each of the accelerometer positions and contained in Tables 9 and 10 are also the frequency variations in percent with reference to the different damage degree. In Figures 25 and 26 the FRF envelope diagrams for the different damage degree *Di*=1,…4 of RC B1 beam with hinged ends, respectively, without and with strengthening are shown.

The beam B3 subjected to bending tests and damaged by cracking of the concrete was subjected to free vibration in two border conditions: free-free and hinged ends. The average values of the frequencies measured for the first four modes for free vibration are indicated in the Table 11 and Table 12, together with the frequency variations in percent, both for RC beam B3 without and with strengthening, assuming free-free ends. Figure 27 shows the FRF envelopes, for the different damage degrees *Di*= 0,1…3, for every position point of the accelerometer, for beam B3 without NSM GFRP strengthening. As it can be seen from the envelope diagrams of FRFs, it is clear that there has been a progressive lowering of the frequency values from the undamaged degree *D0* up to the damage degree *D3*.

The FRF envelope diagrams for the *i*=1,…9 marks for RC beams B3 with NSM GFRP rod at all damage condition *Di*= 0,1…3 are shown in Figure 28. It is possible to observe that

the strengthening by NSM GFRP rod has improved the strength of the beam with a minor decrease of frequency values to the increase of loading conditions.

The experimental data are reported for the same un-strengthened and strengthened B3 beam at the various damage conditions, *Di*, by varying the border condition with hinge constraints (Tabs. 13 and 14). In the Figures 29 and 30 the experimental FRF envelope diagrams are shown for B3 damaged without and with strengthening under different degree conditions *Di* with bending tests.

In the case of hinge-hinge conditions, the translation of the modal peaks towards lower frequencies appears very limited both for the beam without and with NSM GFRP rod, compared to the boundary condition of free-free ends.

Also in this case, the application of the NSM GFRP strengthening has improved the strength of the beam, ensuring that failure is due to loss of compressive strength of concrete.

* * *

Dynamic tests were carried out on RC beam B2 considering two different type of damage: notches on concrete cover and concrete's cracking by bending tests. The experimental response of RC beam model, B2, was analysed using dynamic tests considering free-free ends with the same procedure described above.

The experimental data recorded during the vibrational test were elaborated in frequency domain through the FFT technique and the FRFs were obtained using Pulse software as already mentioned. Table 15 contains the experimental frequency data recorded for the strengthened beam by NSM GFRP rod at the different levels of damage due to notching, together with the frequency variations in percent. The envelope of experimental FRF diagrams at different damage state *Di* i*=1,…,3 recorded by the accelerometer in a number of selected mark points is in Figure 31.

Lastly, the notches were filled with epoxy resin and the strengthened beam B2 with NSM GFRP rod was subjected to bending tests with cyclic loading path. Natural frequency values were measured at each step of loading, *Di* with *i*=0, 1, .., 4. The frequencies measured for the first four modes are indicated in the Table 16 for strengthened RC beam B2 damaged by concrete cracking. It is also reported the frequency variations in percent with reference to the different damage degrees. Figure 32 shows the envelope of FRFs recorded during free vibration tests for each step of damaged degree.

It is noted that the damage by notches produces minor frequency variation compared to those caused by cracking of concrete. This consideration is confirmed by the trend of the envelopes of FRFs, which are reported on Figures 31 and 32.

The variations in percent of frequency values (Tab. 16) are quite similar for four modes of vibration if the beam is subjected to free vibration with free-free ends and with maximum variation of frequency at first mode equal to 22.73%.

From Figure 31 it emerges that the maximum frequency values are not appreciably distinguishable as confirmed by the low variations of frequency shown in Table 15 for damage due to notches.

4. Discussion

Investigation on RC beams strengthened by NSM GFRP rod allows the definition of a number of aspects that can be useful in practice. The first result that needs to be underlined is the adequate behaviour of the NSM GFRP rod strengthening in terms of maintaining of adherence without detachment until the ultimate strain of compressive concrete. During the static tests we obtained an increment of stiffness of beams with NSM GFRP rod at the same cyclic bending loads compared to the unstrengthened RC beams; a reduction of de-

flection and a value of ductility ratio deduced by the ratio of ultimate curvature value, χ_u, on yield curvature, χ_y, greater that $\chi_u/\chi_y > 5$.

The vibration analysis as non-destructive method of control of RC unstrengthened and strengthened is convenient. Considering the dynamic response of tested beams it can be noted that, in general, increase in damage reduces frequency values for the all first four modes of vibration r= 1,…,4 although the results are more significant when the border condition are free-free ends.

Further, it may be useful to compare the variations of frequency values $\frac{\Delta f_r}{f_{r,exp}^{D0}} = 100\frac{f_{r,exp}^{D0} - f_{r,exp}^{Di}}{f_{r,exp}^{D0}}$, in percent, for unstrengthened and strengthened beams under the different loading conditions expressed by bending moment M/M_{max} ratios (Figure 33(a) and (b)). The comparison of frequency variations for the response for first two modes i=1,2 versus the ratio of bending moment M/M_{max} when the beams B1 and B3 are strengthened, shows that the variations of frequency values is rather small. In fact, the strengthening by NSM GFRP rod contributes to reducing the width of the cracks undergoing even heavy loads. These diagrams confirm that the decrease of frequency values correlated to increase of bending moment is relevant for a non-strengthened beam while the diagrams in Figures 33 are substantially constant in the case of RC beams strengthened by NSM GFRP rod.

Finally, another result obtained by investigation is that the Bernoulli's hypothesis may be not applied in the calculus of RC section strengthened with NSM GFRP rod because the section does not remain plane under bending with a *stress-strain lag* of GFRP rod already recorded at the elastic phase as shown in Figures 10 and 21.

In Table 17 the ratios $k_1 = \frac{\varepsilon_{GFRP}}{\varepsilon_s}$ and $k_2 = \frac{\varepsilon^*_{GFRP} - \varepsilon_{GFRP}}{\varepsilon^*_{GFRP}}$, where $\varepsilon^*_{\mathrm{GFRP}}$ is the strain that GFRP rod should have with the Bernoulli's hypothesis of plane section, are shown. These ratios have been evaluated for damage degrees D1 to D3 thus until values of steel strain

greater than yield strain of steel reinforcement both for the RC beams B1 and B3. It may be noted that the average ratios are quite constant with average values $k_{1,av} \cong 0.66$ and $k_{2,av} \cong 0.46$, so that in the analysis of RC beams strengthened by NSM GFRP rods, it is convenient to adopt the coefficient $k_{1,av}$ (or $k_{2,av}$) to avoid to overestimate the strength of beams.

5. Conclusions

The investigation on three RC beams damaged and strengthened with NSM GFRP rod allowed to obtain useful results below summarized:

1. The NSM GFRP rod strengthening technique may be adequate, without loss of adherence of GFRP rod with the concrete cover up to failure of RC beams due to bending tests;
2. The analysis of free vibration of the beams damaged by cracking of the concrete and strengthened using NSM GFRP rod highlights that strengthening increases stiffness of RC beam and limits the damage state under bending conditions with limited frequency variations even for high bending moment values;
3. Damage due to notches in concrete's compressed zone of RC beams strengthened with NSM GFRP rod is low influent on the dynamic response of beam until failure;
4. Experimental results confirm that it isn't possible to adopt the Bernoulli's hypothesis in the calculus of RC section strengthened with NSM GFRP rod; the section is not plane due to *stress-strain lag* of GFRP rod that can be estimate considering average strain ratios k_1 (or k_2) evaluated by experimental data.

Acknowledgement

This experimental research was supported by research funds provided by Università Politecnica delle Marche. The authors would like to express their gratitude to all the technicians and students who collaborated to develop the experimental research.

NOTATION

^{U}, ^{D} = index for undamaged state; index for damaged state
f_c = compressive strength of concrete
E_c = Young's modulus of concrete
f_y = yield strength of steel reinforcements
E_s = Young's modulus of steel reinforcements
E_{adh} = Young's modulus of epoxy resin
v_{adh} = Poisson's coefficient of epoxy resin
Di = damage degree for cracking of concrete
ε_s = steel strain
ε_c = concrete strain
ε_{GFRP} = GFRP strain
M = bending moment
χ = curvature
P = load
δ = deflection at midspan
A = cross section area of beam
ρ = density
EI = bending stiffness of beam
I = moment of inertia of beam
ω = circular frequency value; angle of phase
λ = eigenvalue
Di^* = damage degree by notch
f, Δf = frequency value; difference between undamaged and damaged frequencies
k_1, k_2 = coefficient of *stress-strain lag* of GFRP

References

1. Meier U. Bridge repair with high performance composite materials. Material und Technick 1987; **4**:125-128.
2. MPA. Bonding of Steel and GFRP Plates in the area of Coupling Joints. Talbrucke Hattenbusch. Federal Institute for Materials Testing, Braunschwerg, Res. Report Nº3126/1429, 1987.
3. Saadatmanesh H., Ehsani M.R. RC beams strengthened with GFRP plates. I: experimental study. Journal of structural engineering 1991; **117**(11): 3417-3433.
4. Plevris N., Triantafillou T.C. Strengthening of RC beams with epoxy-bonded fibre composite materials. Materials and Structures 1992; **25**: 201-211.
5. Arduini M, Di Tommaso A., Nanni A. Brittle failure in FRP plate and sheet bonded beams ACI Structural Journal 1997; **94**(4): 363-370.
6. Michaluk C.R., Rizkalla S.H., Tadros G., Benmokrane B. Flexural behaviour of one-way concrete slabs reinforced by fibre reinforced plastic reinforcements. ACI Structural Journal 1998; **95**(3): 353-365.
7. An W., Saadatmanesh H., Ehsani M.R. RC beams strengthened with FRP plates. II: analysis and parametric study. J. of Structural Eng. 1991; **117**(11): 3434-3455.
8. Ross C.A., Jerome D.M., Tedesco J.W., Huges M.L. Strengthening of reinforced concrete beams with externally bonded composite laminates. ACI Structural Journal 1999; **96**(2): 212-220.
9. Malek A.M., Saadatmanesh H. Analytical study of reinforced concrete beams strengthened with web-bonded fibre reinforced plastic plates or fabric. ACI Structural Journal 1998; **95**(3): 343-352.
10. Malek A.M., Saadatmanesh H., Ehsani M.R. Prediction of failure load of RC beams strengthened with FRP plate due to stress concentration at the plate end. ACI Structural Journal 1998; **95**(1): 142-152.
11. El-Hacha R., Rizkalla S. Near-surface mounted fibre reinforced polymer reinforcements for flexural strengthening of concrete structures. ACI Structural Journal 2004; **101** (5): 717-726.
12. De Lorenzis L., Teng J.G. Near-Surface mounted FRP reinforcement: an emerging technique for strengthening structures. Composites Part B: Eng. 2007; **38**: 119-143.
13. Capozucca R. Static and dynamic response of damaged RC beams strengthened with NSM CFRP rods. Composite Structures 2009; **91**: 237-248.
14. Sena Cruz J.M., Barros J.A. O., Gettu R., Azevedo A.F.M. Bond behavior of near-surface mounted CFRP laminate strips under monotonic and cyclic loading. ASCE, Journal of Composites for Construction 2006; **10**: 295-303.
15. Sharaky I.A., Torres L., Baena M., Miàs C. An experimental study of different factors affecting the bond of NSM FRP bars in concrete. Composite Structures 2013; **99**: 350-365.
16. Capozucca R. Analysis of bond-slip effects in RC beams strengthened with NSM CFRP rods. Composite Structures, 2013; **102**: 110-123.

17. Capozucca R., Bossoletti S., Montecchiani S. Assessment of RC beams with NSM CFRP rectangular rods damaged by notches. Composite Structures, 2015, **128**: 322-341.
18. Capozucca R. On the strengthening of RC beams with near surface mounted GFRP rods. Composite Structures, 2014, **117C**: 143-155.
19. Ding Y., Ning X., Zhang Y., Pacheco-Torgal F., Aguiar J.B. Fibres for enhancing of the bond capacity between GFRP rebar and concrete. Construction and Building Materials 2014, **51**:303-312.
20. Masmoudi A., Ouezdou M. Ben, Bouaziz J. New parameter design of GFRP RC beams. Construction and Building Materials 2012, **29**: 627-632.
21. Mansouri L., Djebbar A., Khatir S., Ali H.T., Behtani A., Wahab M.A. Static and fatigue behaviors of short glass fiber–reinforced polypropylene composites aged in a wet environment. Journal of Composite Materials 2019, **53**(23): 3629-3647.
22. Mansouri L., Djebbar A., Khatir S., Wahab M.A. Effect of hygrothermal aging in distilled and saline water on the mechanical behaviour of mixed short fibre/woven composites. Composite Structures 2019, **207**(1): 816-825.
23. Capozucca R. Vibration analysis of damaged RC beams strengthened with GFRP. Composite Structures, 2018, 200: 624-634.
24. Capozucca R. A reflection on the application of vibration tests for the assessment of cracking in PRC/RC beams. Engineering Structures, 2013, **48**: 508-518.
25. Salawu O.S. Detection of structural damage through changes in frequency: a review. Engineering Structures, 1997, 120: 2437-2450.
26. Khatir S., Brahim B., Capozucca R., Wahab M.A. Damage detection in CFRP composite beams based on vibration analysis using proper orthogonal decomposition method with radial basis functions and cuckoo search algorithm. Composite Structures 2018, **187**(1): 344-353.
27. Khatir S., Tiachacht S., Thanh C.-L., Bui T.Q., Wahab M.A. Damage assessment in composite laminates using ANN-PSO-IGA and Cornwell indicator. Composite Structures 2019, **230**(15): 111509.
28. Khatir S., Wahab M.A. Fast simulations for solving fracture mechanics inverse problems using POD-RBF XIGA and Jaya algorithm. Engineering Fracture Mechanics 2019, **205**:285-300.
29. Khatir S., Wahab M.A., Boutchicha D., Khatir T. Structural health monitoring using modal strain energy damage indicator coupled with teaching-learning-based optimization algorithm and isogoemetric analysis. Journal of Sound and Vibration 2019, **448**(26): 230-246.
30. Zenzen R., Belaidi I., Khatir S., Wahab M.A. A damage identification technique for beam-like and truss structures based on FRF and Bat Algorithm. Comptes Rendus Mècanique 2018, **346**(12): 1253-1266.
31. Tiachacht S., Bouazzouni A., Khatir S., Wahab M.A., Behtani A., Capozucca R. Damage assessment in structures using combination of a modified Cornwell indicator and genetic algorithm. Engineering Structures 2018, **177**(15): 421-430.

32. ASTM D 3039/D 3039 M - 08. Standard Test Method for Tensile Properties of Polymer Matrix Composite Materials. American Standard of Testing and Materials, 2008.
33. Warburton G.B. The dynamical behaviour of structures. Pergamon Press, 1964, Oxford.

List of Figures:

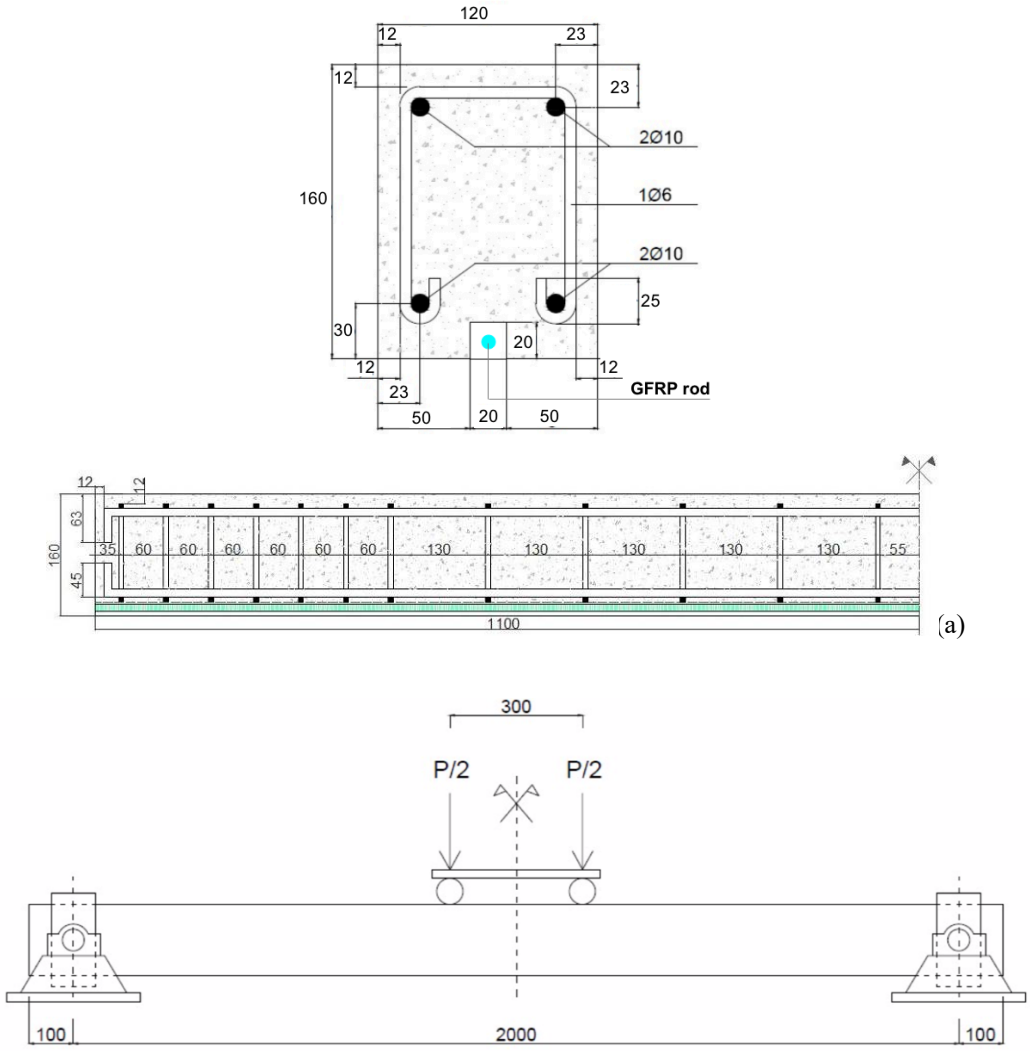

(b)

Fig. 1 - (a) Geometric dimensions of RC beams with steel reinforcement and NSM GFRP rod; (b) set up of bending tests.

Figure 2 – Compression test of prismatic specimen of adhesive material.

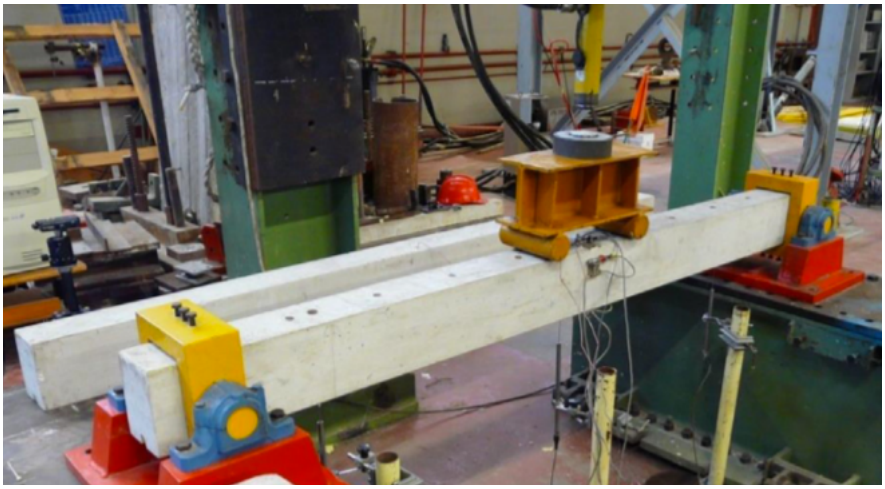

Figure 3 – Set up of simply supported beam B1 with hinge restraints under static bending tests.

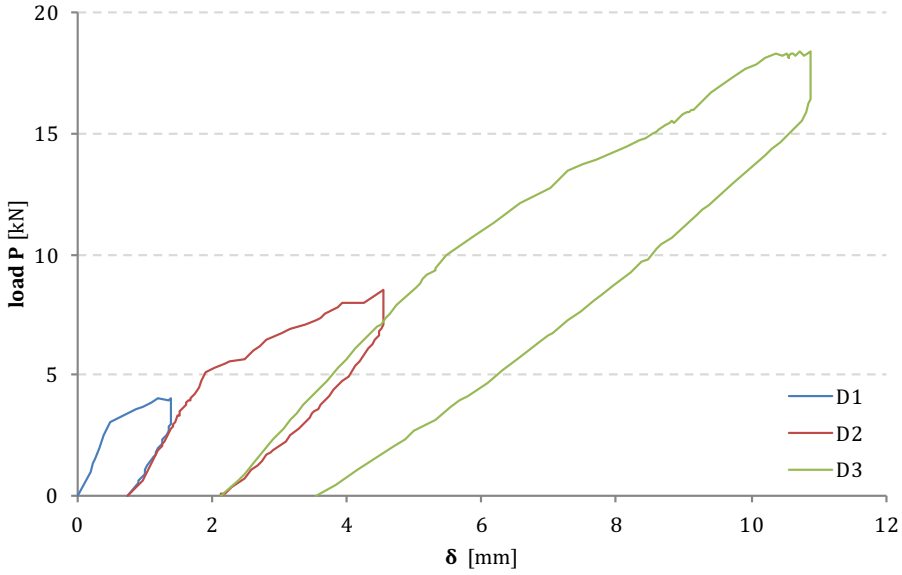

(a)

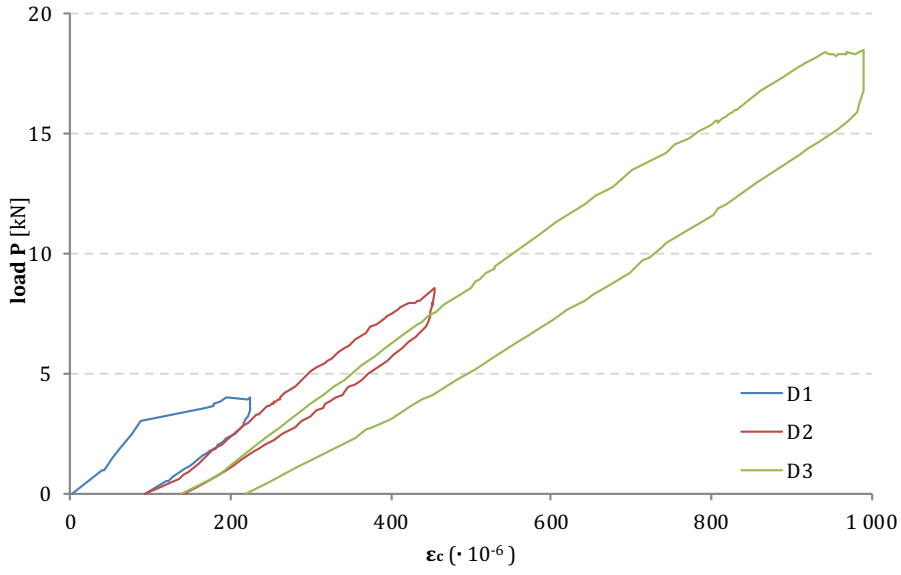

(b)

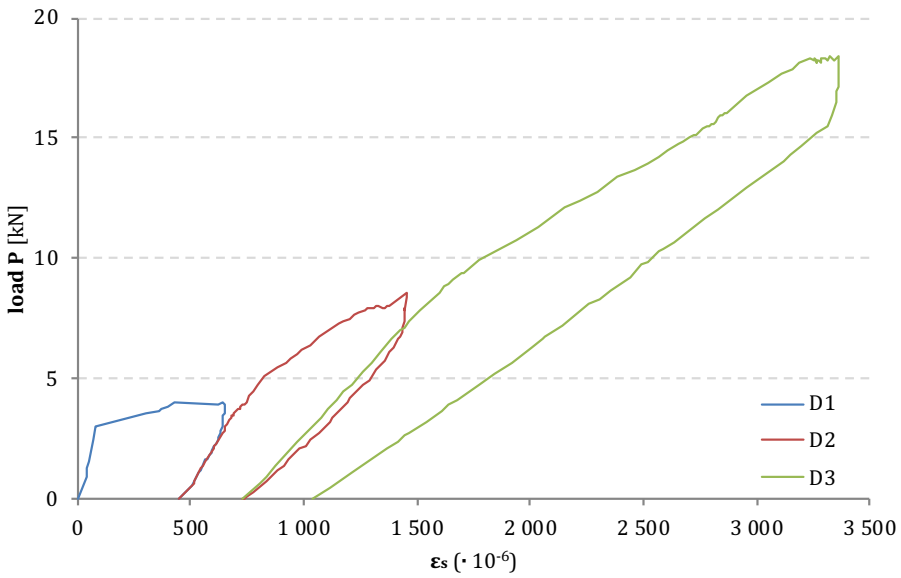

(c)

Figure 4 – (a) Exp. diagram load, P, vs deflection, δ, at midspan of RC beam B1; (b) exp. diagram load, P, vs strain of concrete, ε_c, at the edge of compressive concrete; (c) exp. diagram load, P, vs strain of steel, ε_s.

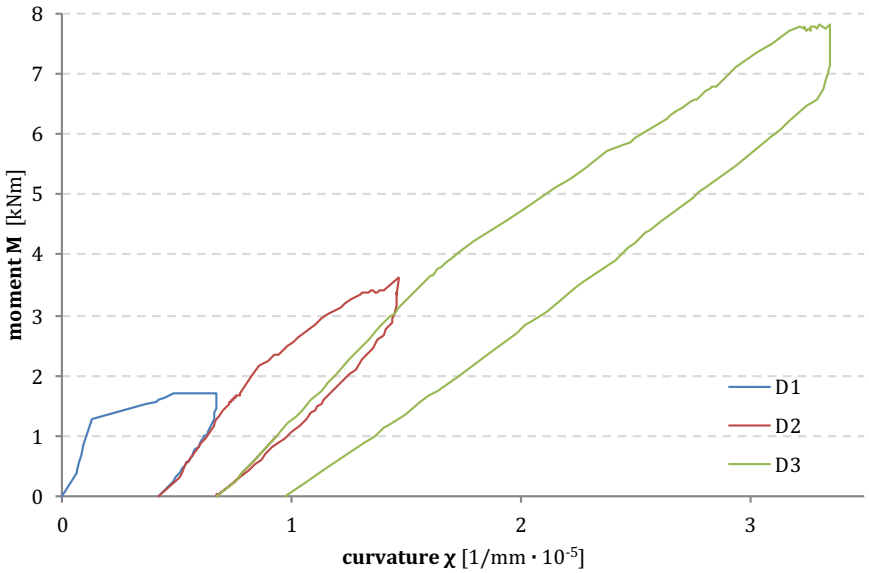

Figure 5 – Exp. diagram moment, M, vs curvature, χ, at the midspan section of RC beam B1.

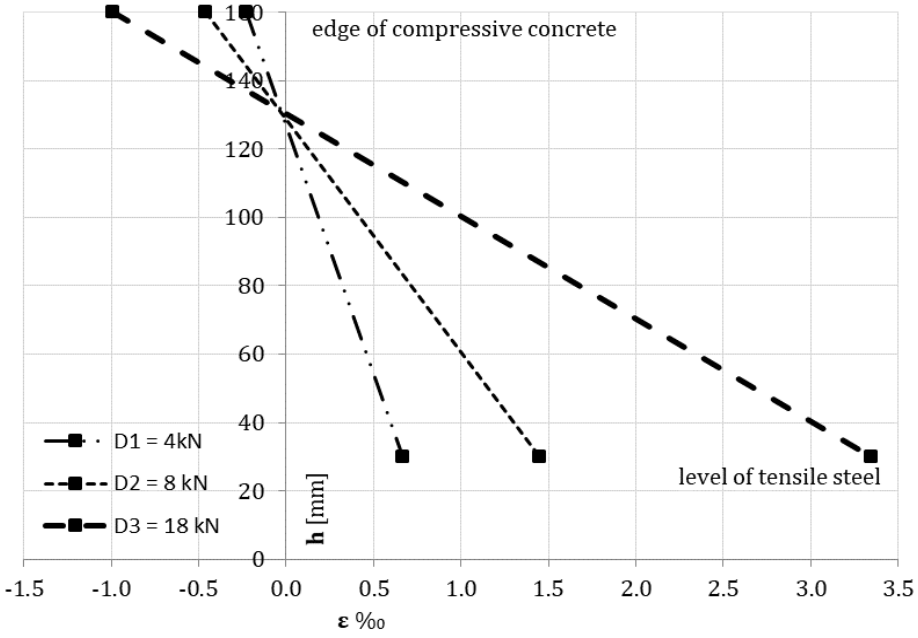

Figure 6 – Exp. strain values vs height of midspan section at different cycles of loading (*Di* with *i*=1,…,3) for un-strengthened beam B1.

D1

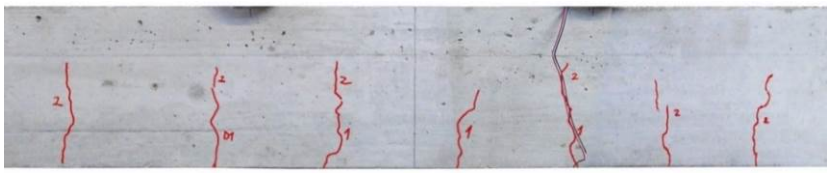

D2

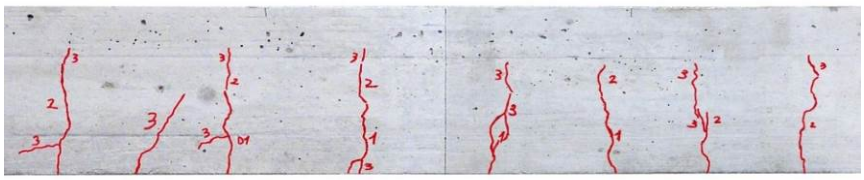

D3

Figure 7 - Cracking damage development due to bending test at different damage degrees *Di*, *i*=1,2,3 for RC beam B1.

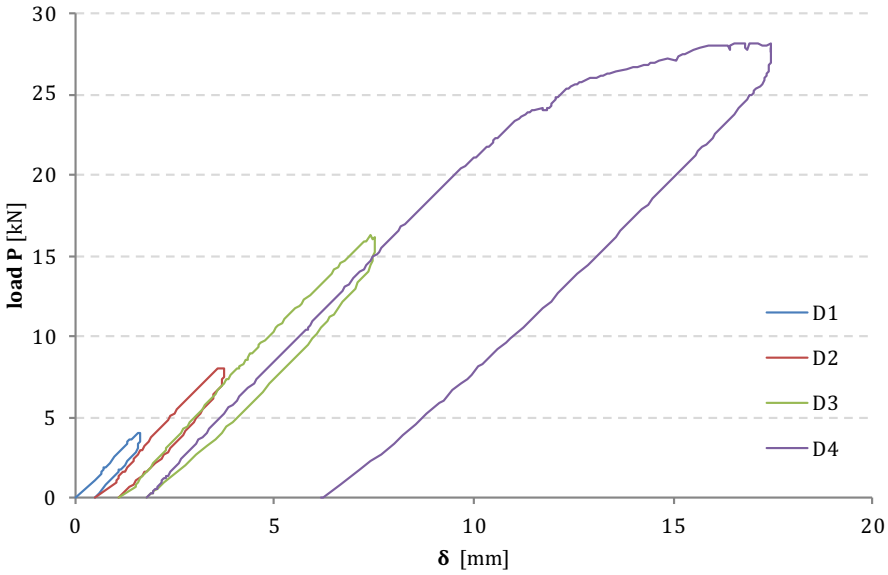

(a)

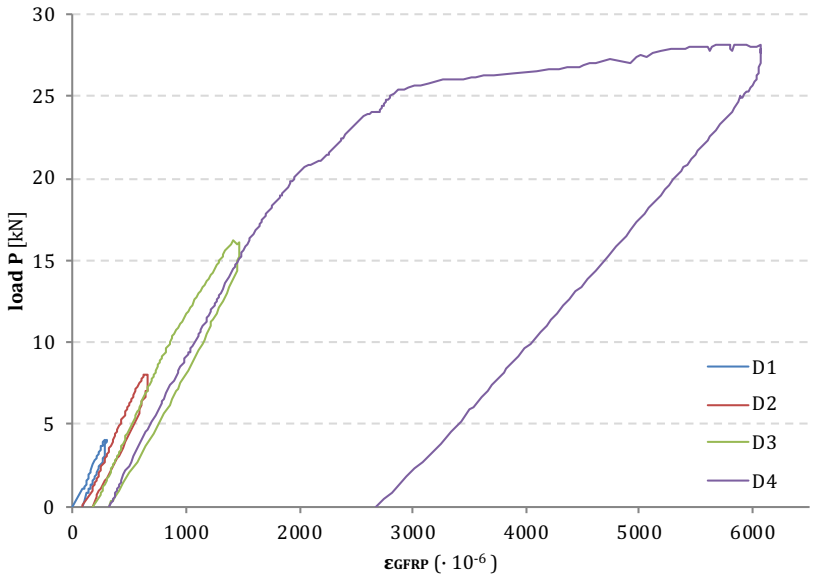

(b)

Figure 8 – (a) Exp. diagram load, P, vs deflection, δ, at the midspan of strengthened beam B1; (b) exp. diagram load, P, vs strain of GFRP rod, ε_{GFRP}.

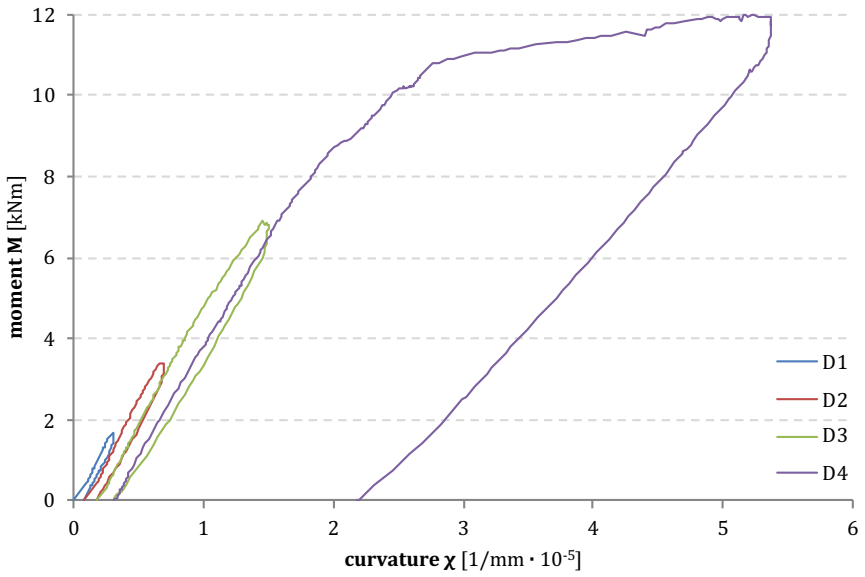

Figure 9 – Exp. diagram moment, M, vs curvature, χ, at the midspan section of strengthened beam B1.

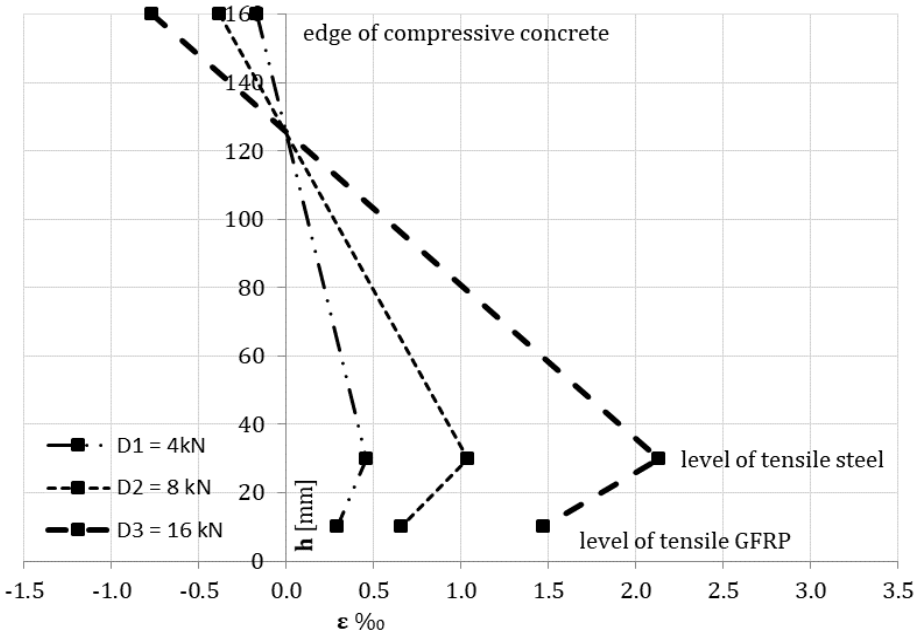

Figure 10 – Exp. strain values vs height of midspan section at different cycles of loading (*Di* with *i*=1,…,3) for strengthened beam B1.

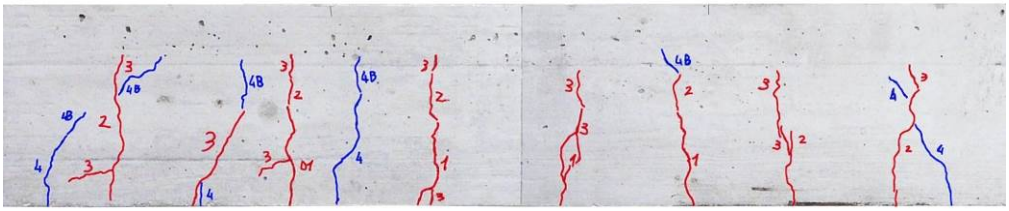

Figure 11 – Cracks on beam B1 strengthened with NSM GFRP rod (damage degree *D4*).

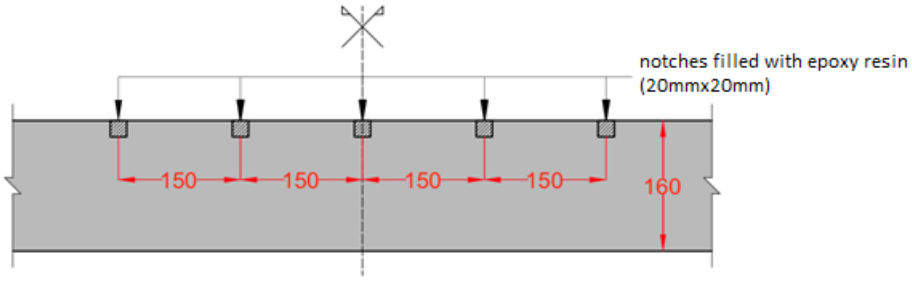

(a)

(b)

Figure 12 – (a) Beam B2 damaged by notches at concrete cover and repaired with epoxy resin (damage degree *D3**); (b) strain-gauges on resin and concrete at the extrados of the midspan section.

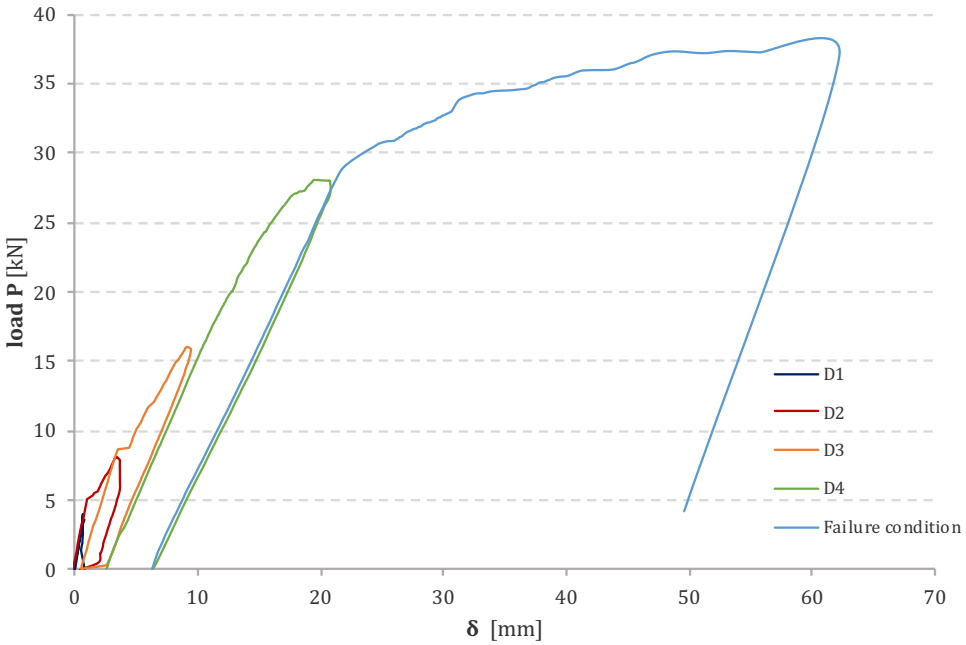

(a)

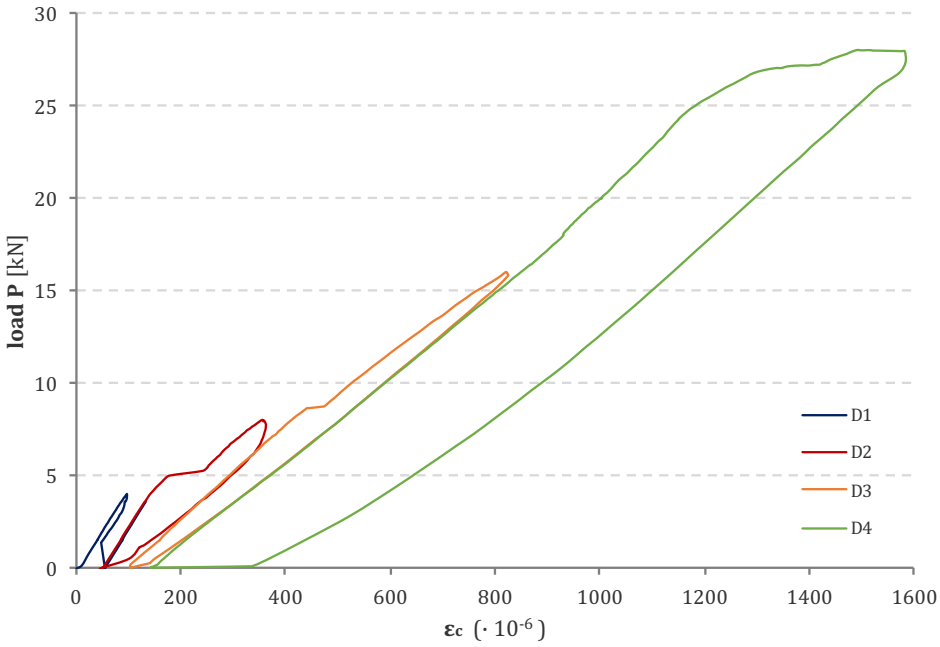

(b)

Figure 13 – (a) Exp. diagram load, P, vs deflection, δ, at the midspan section of strengthened beam B2; (b) exp. diagram load, P, vs strain of concrete, ε_c, at the edge of compressive concrete.

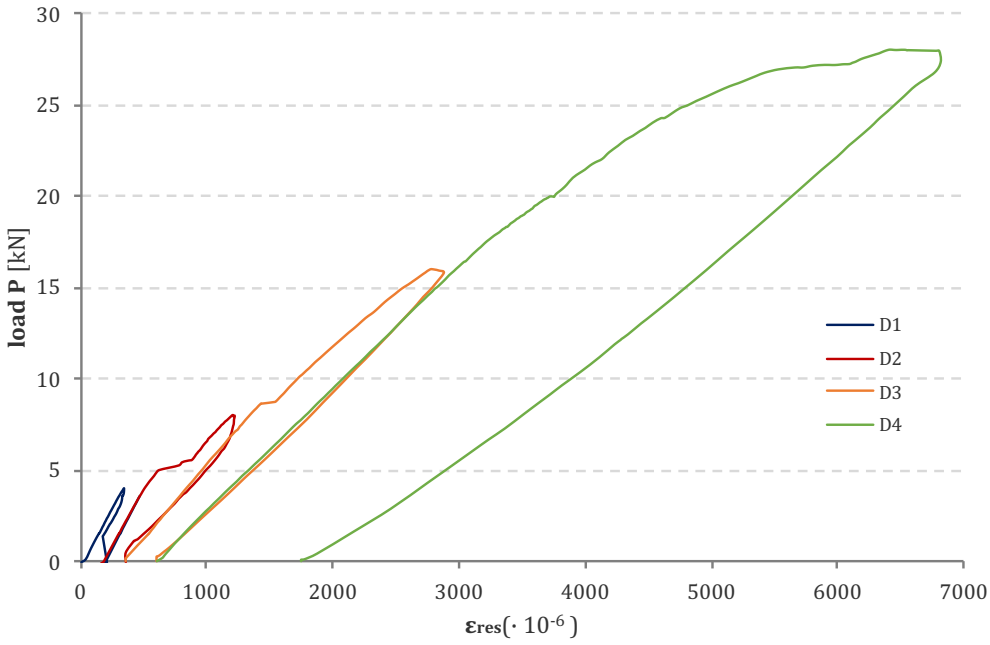

Figure 14 – Exp. diagram load, P, vs strain of resin, ε_{res}, for strengthened beam B2.

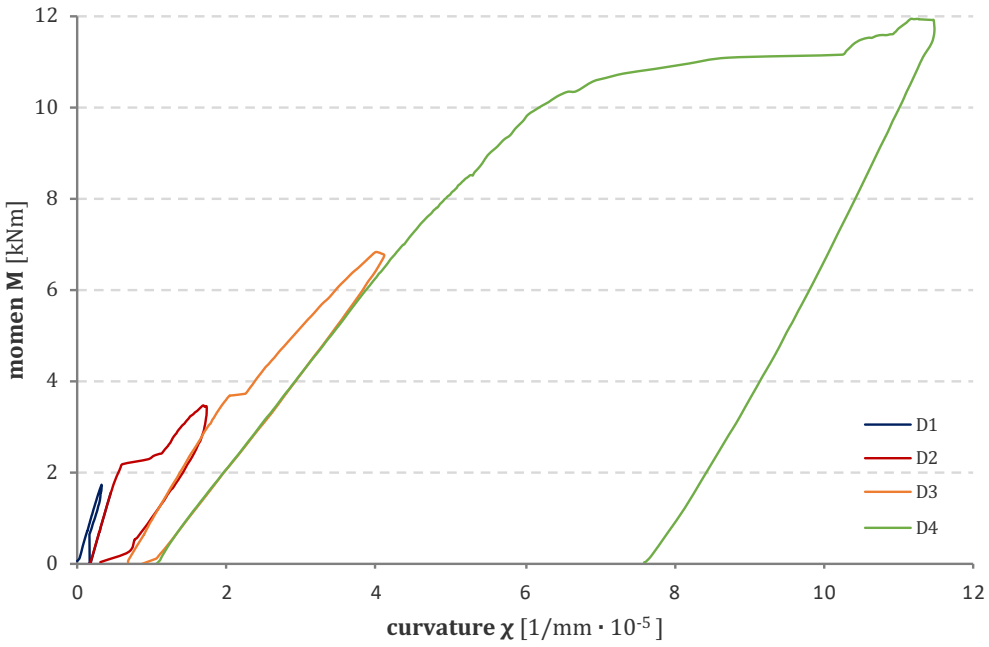

Figure 15 – Exp. diagram moment, M, vs curvature, χ, at the midspan section of strengthened beam B2.

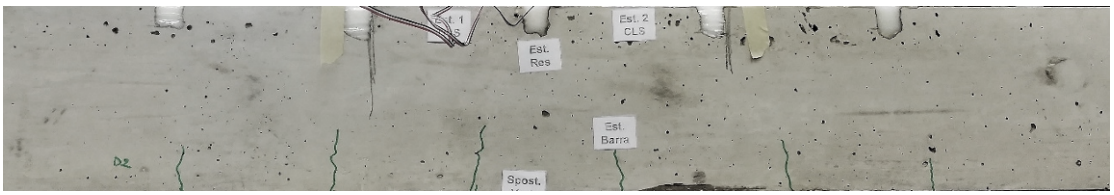

D2

D3

Figure 16 – Cracking damage development due to bending test at different damage degrees Di, i=2,3 for strengthened RC beam B2.

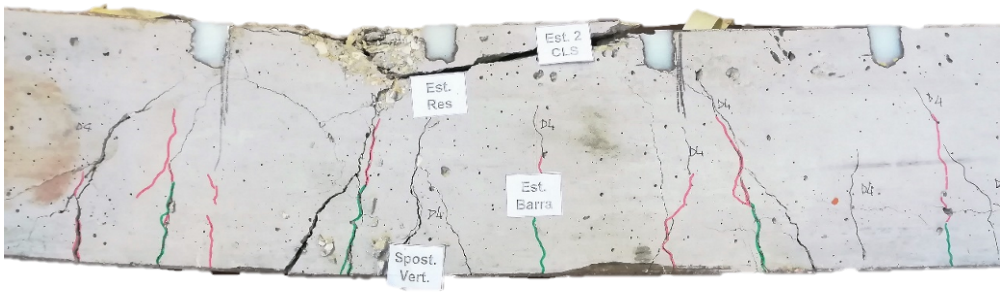

Figure 17 – View of failure of strengthened beam B2.

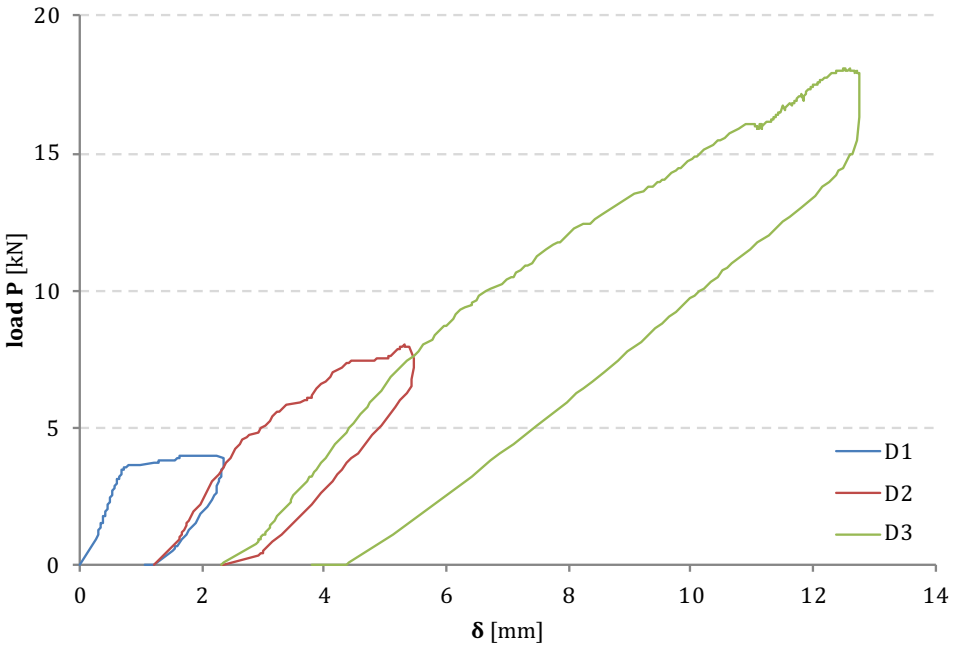

Figure 18 – Experimental diagram load, *P*, vs deflection, δ, at midspan on RC beam B3.

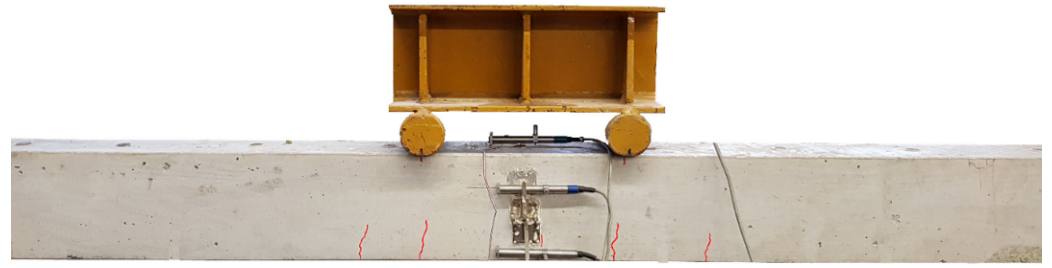

D1

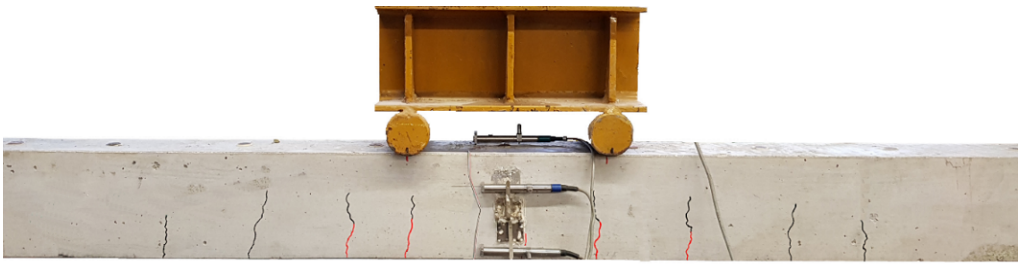

D2

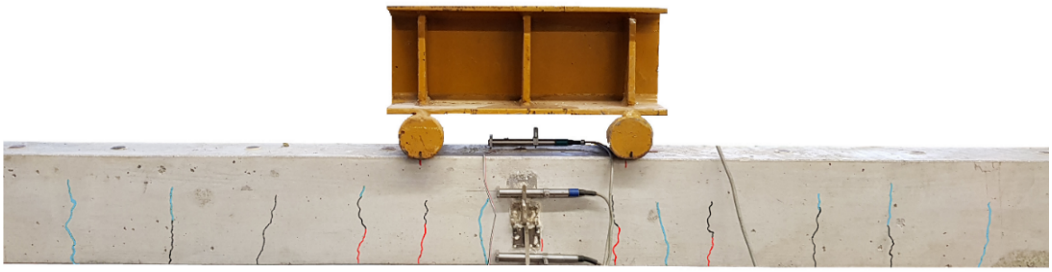

D3

Figure 19 – Cracking damage development due to bending test at different damage degrees *Di*, *i*=1,2,3 for RC beam B3 without NSM GFRP rod.

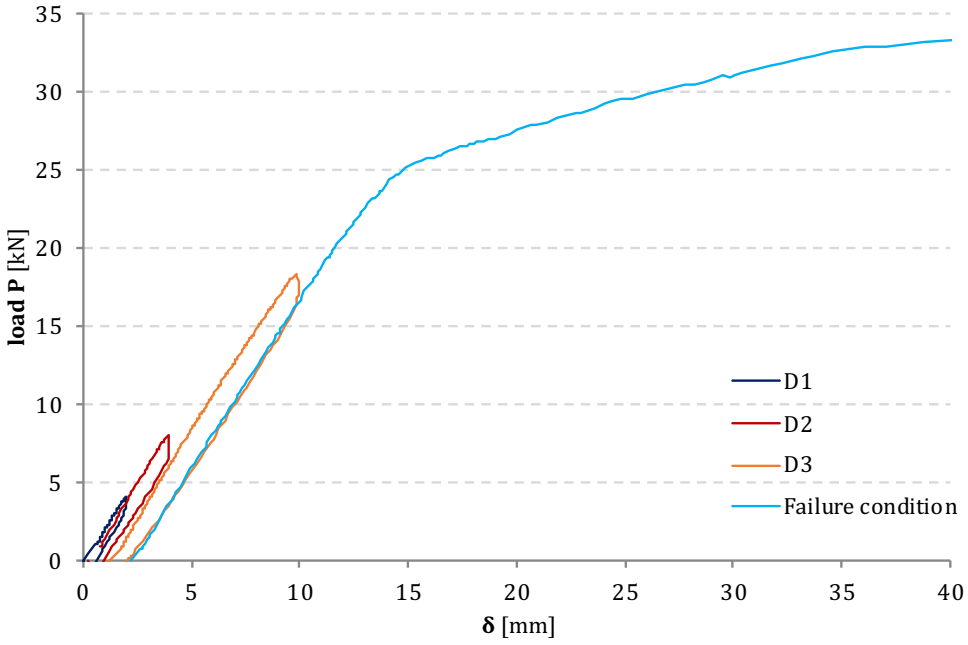
load P [kN]
δ [mm]
D1
D2
D3
Failure condition

(a)

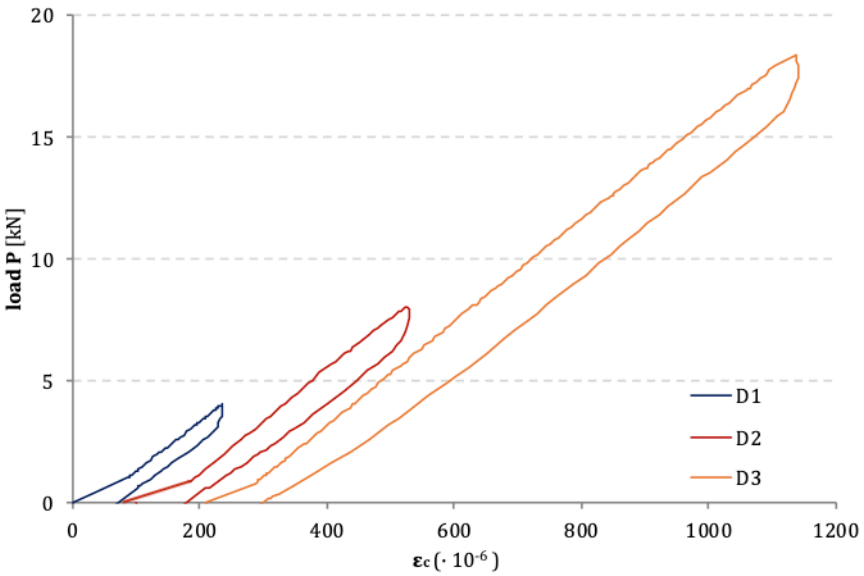
load P [kN]
εc (· 10-6)
D1
D2
D3

(b)

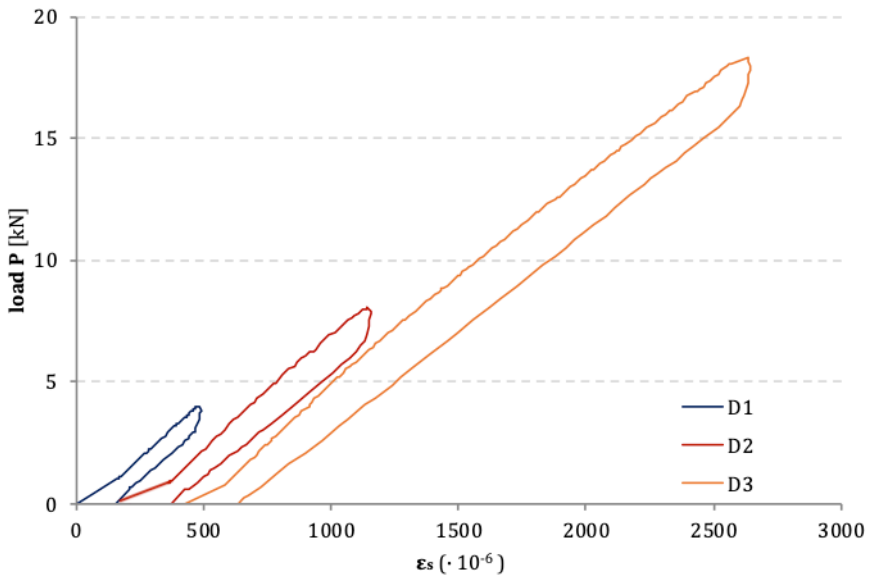

(c)

Figure 20 – (a) Exp. diagram load, P, vs deflection, δ, at midspan of strengthened beam B3; (b) exp. diagram load, P, vs strain of concrete, ε_c, at the edge of compressive concrete; (c) exp. diagram load, P, vs strain of steel, ε_s.

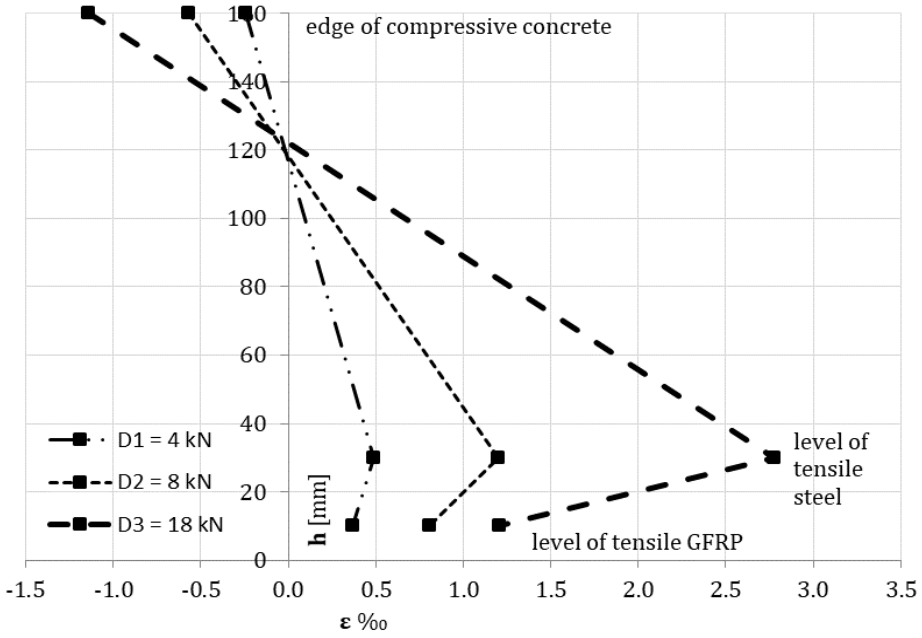

Figure 21 – Exp. strain values vs height of midspan section at different cycles of loading (*Di* with *i*=1,…,3) for strengthened beam B3.

Figure 22 – Collapse view of strengthened beam B3 ($P \cong 33$ kN).

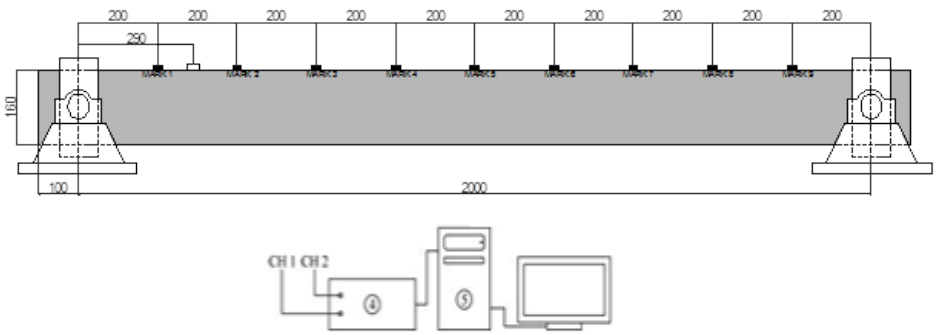

1. beam 2. accelerometer 3. impact hammer 4. analyzer FFT 5. PC

(a)

(b) (c)

Figure 23 – (a) Set up of vibration tests on undamaged RC beams with hinge-hinge condition and instrumentation for dynamic tests; (b) beam hung to elastic springs and (c) accelerometer.

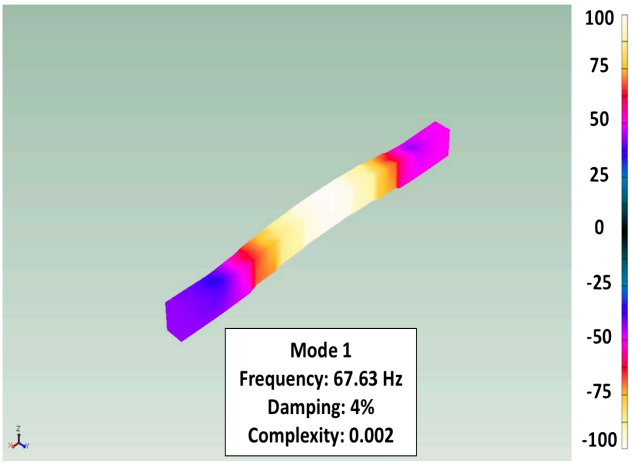

I mode (67.63 Hz)

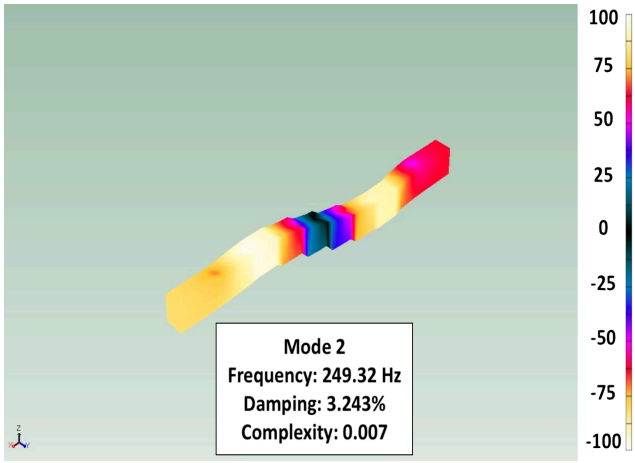

II mode (249.32 Hz)

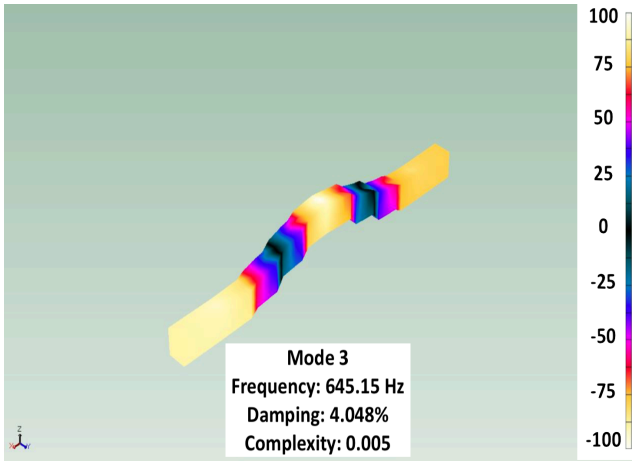

III mode (645.15 Hz)

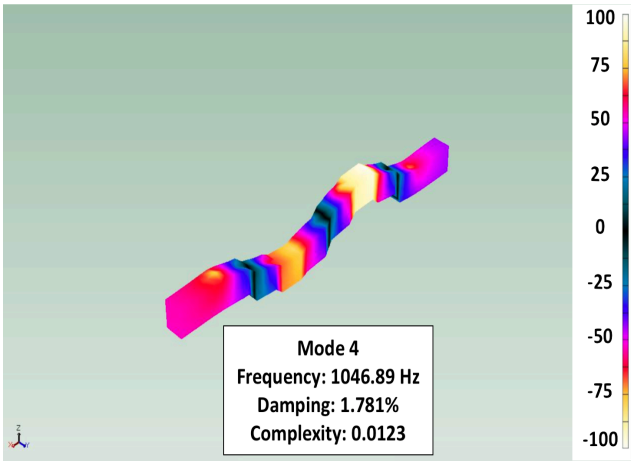

IV mode (1046.89 Hz)

Figure 24 – Modal shapes of free vibration of undamaged RC beam B3.

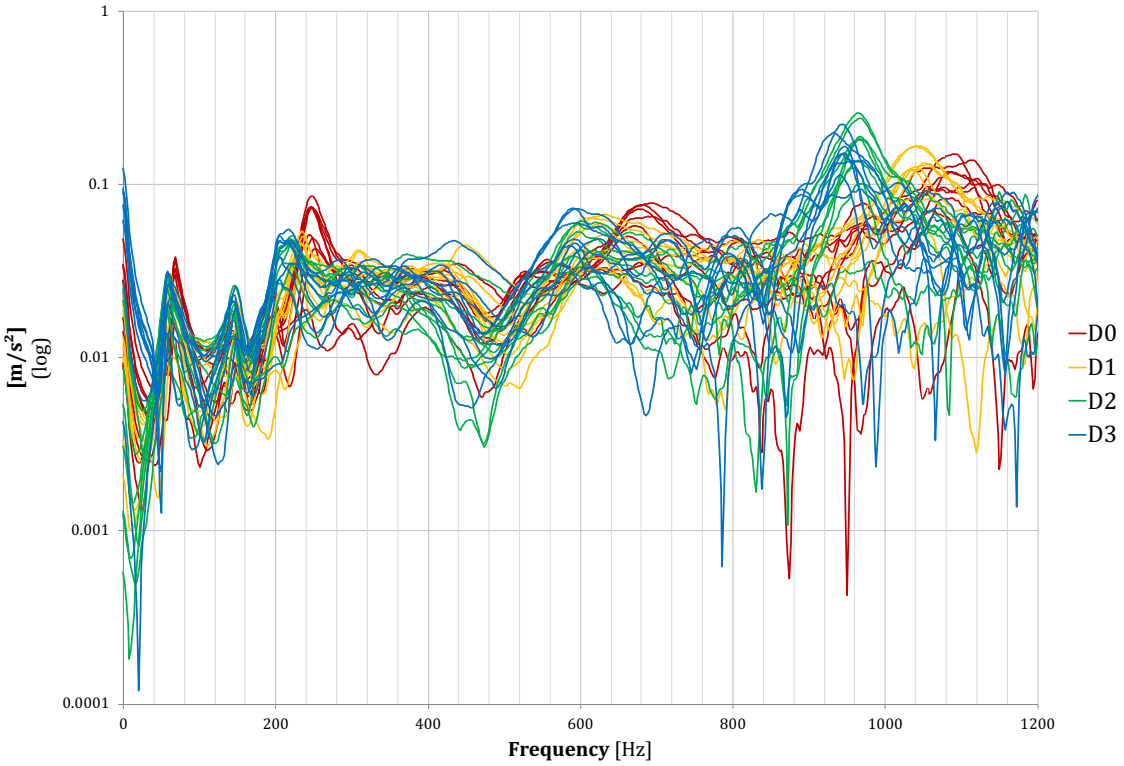

Figure 25 –Envelope of FRFs for un-strengthened beam B1 with hinge-hinge ends at different damage degrees *Di*=0, 1,…, 3.

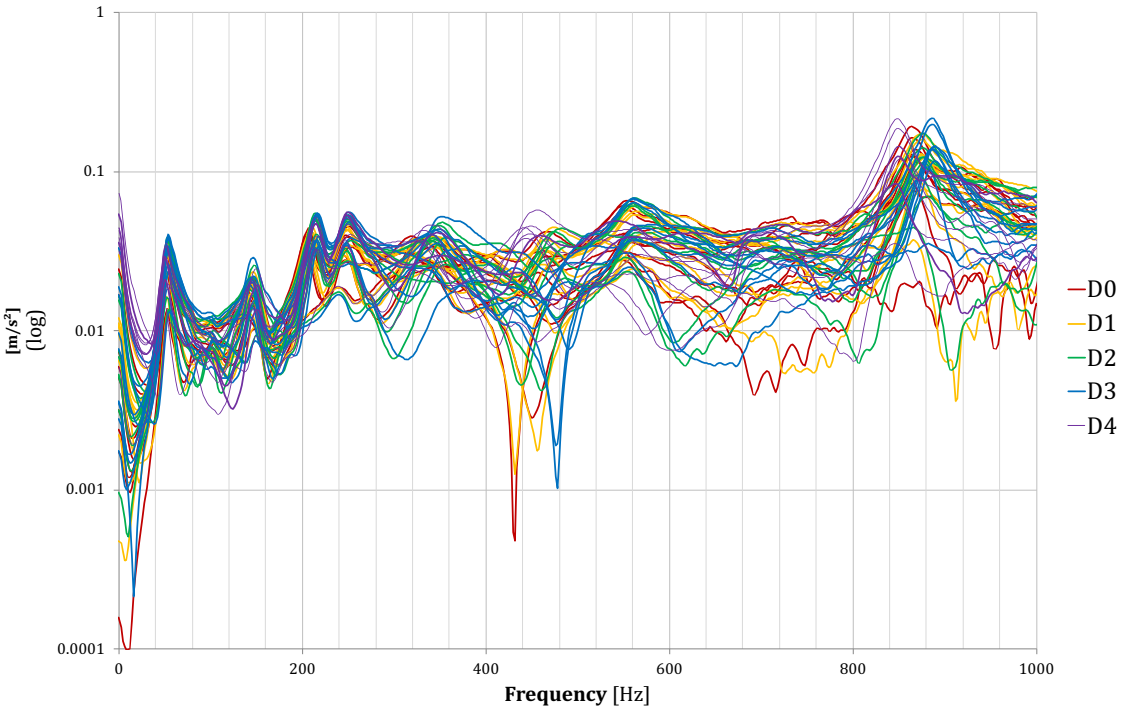

Figure 26 – Envelope of FRFs for strengthened beam B1 with hinge-hinge ends at different damage degrees *Di*=0, 1, …, 3.

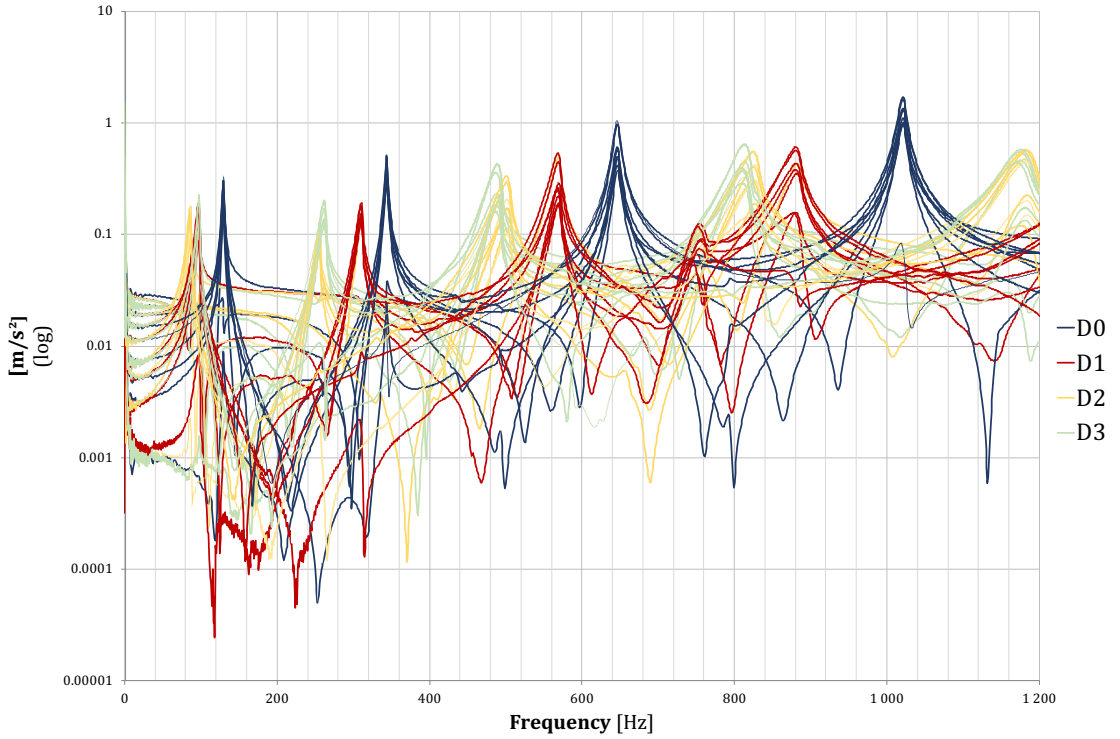

Figure 27 – Envelope of FRFs for un-strengthened beam B3 with free-free ends at different damage degrees *Di*=0, 1…, 3.

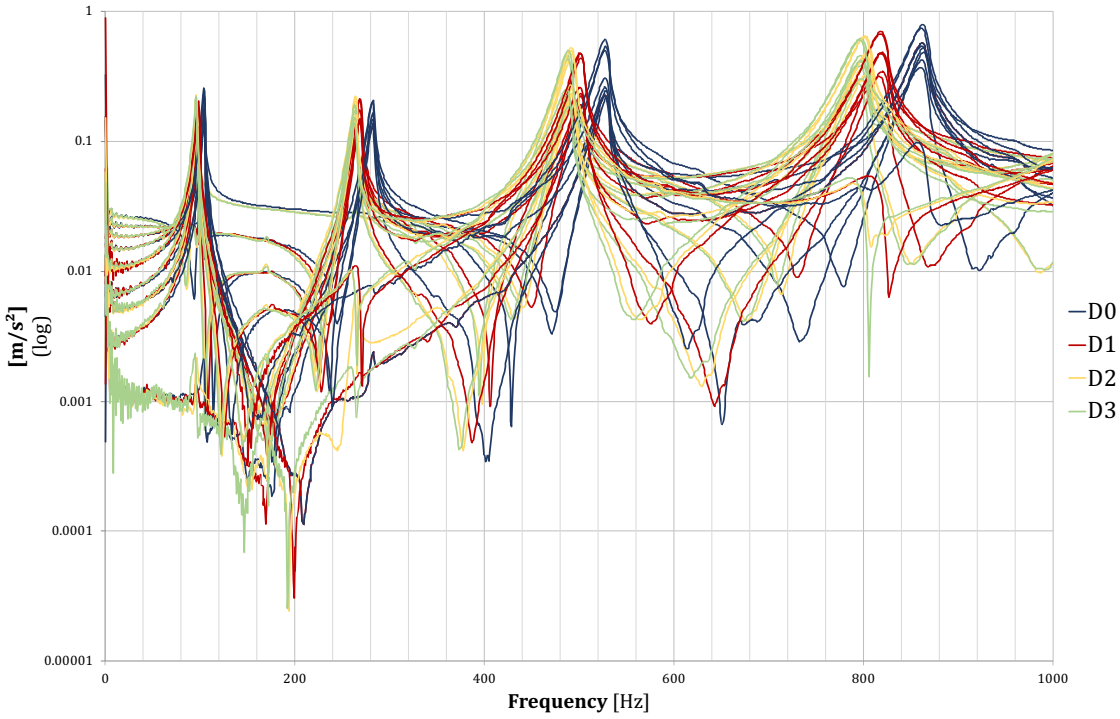

Figure 28 – Envelope of FRFs for strengthened beam B3 with free-free ends at different damage degrees *Di*=0, 1,…, 3.

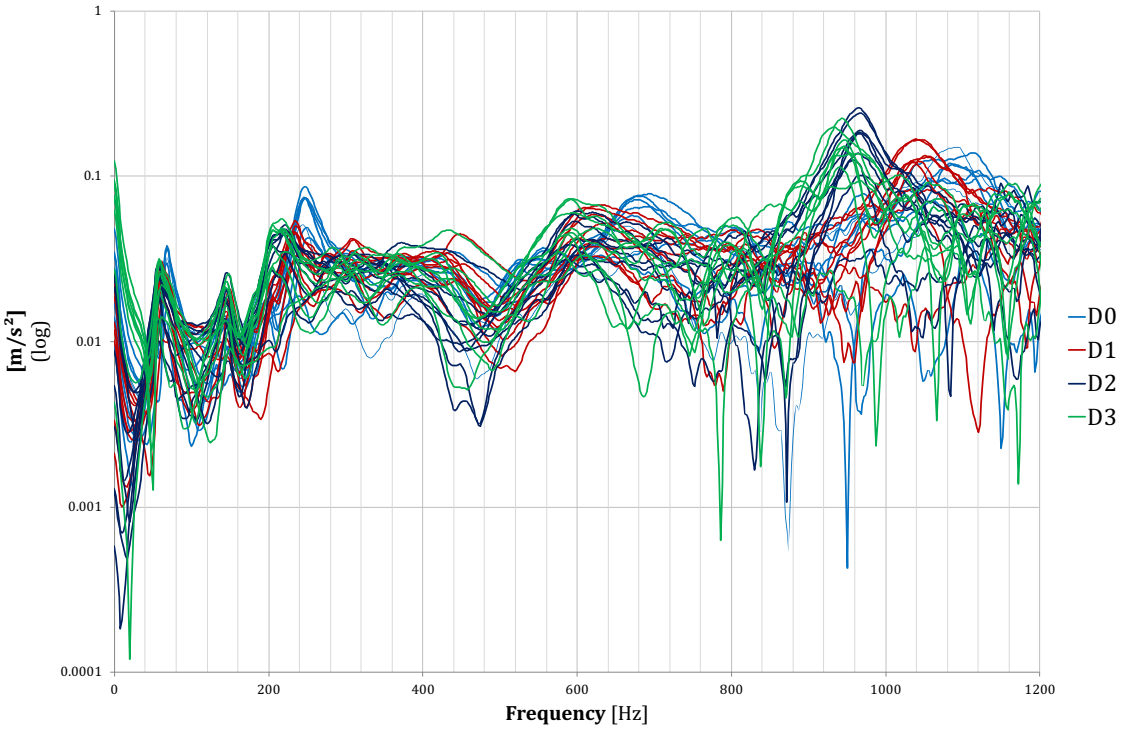

Figure 29 – Envelope of FRFs for un-strengthened beam B3 with hinge-hinge ends at different damage degrees *Di*=0, 1, …, 3.

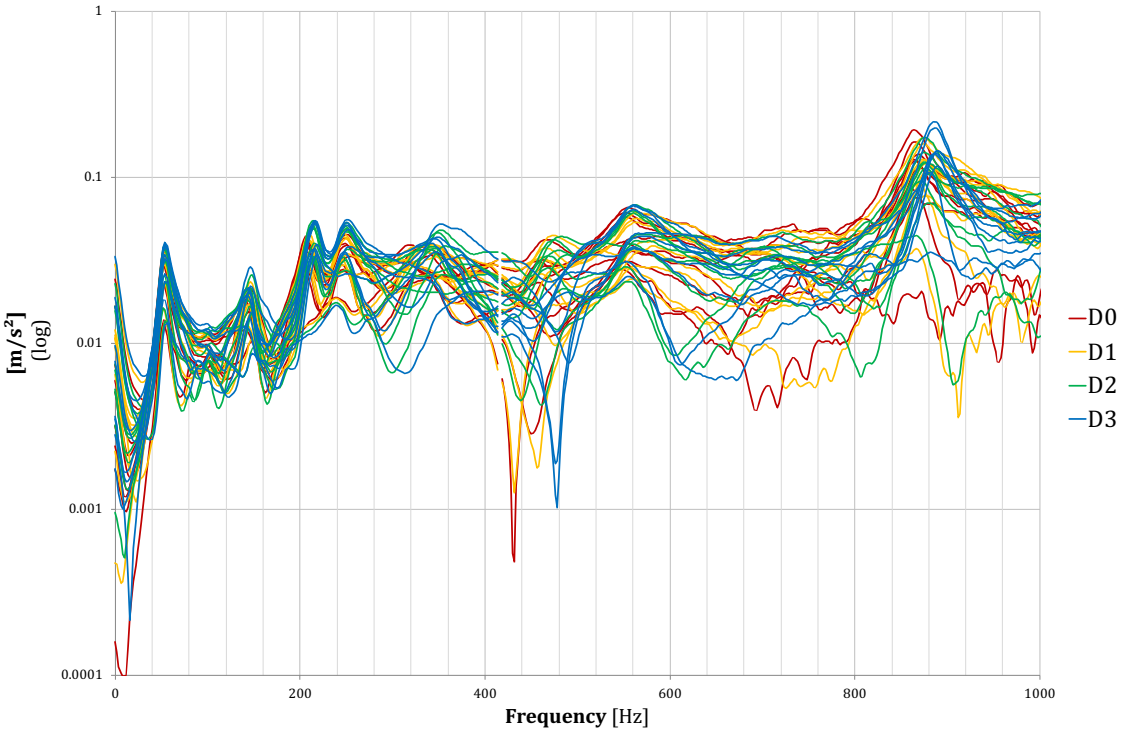

Figure 30 – Envelope of FRFs for strengthened beam B3 with hinge-hinge ends at different damage degrees *Di*=0, 1,…, 3.

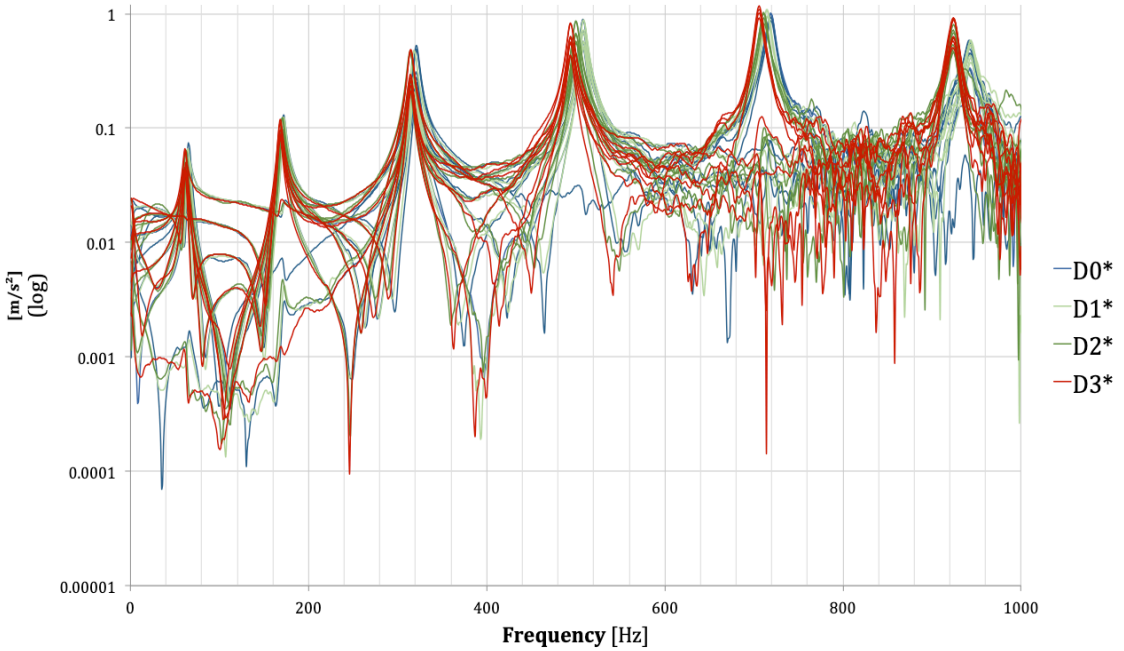

Figure 31 – Envelope of FRFs for strengthened beam B2 with free-free ends at different damage degrees *Di**=0, 1,…, 3 by notches.

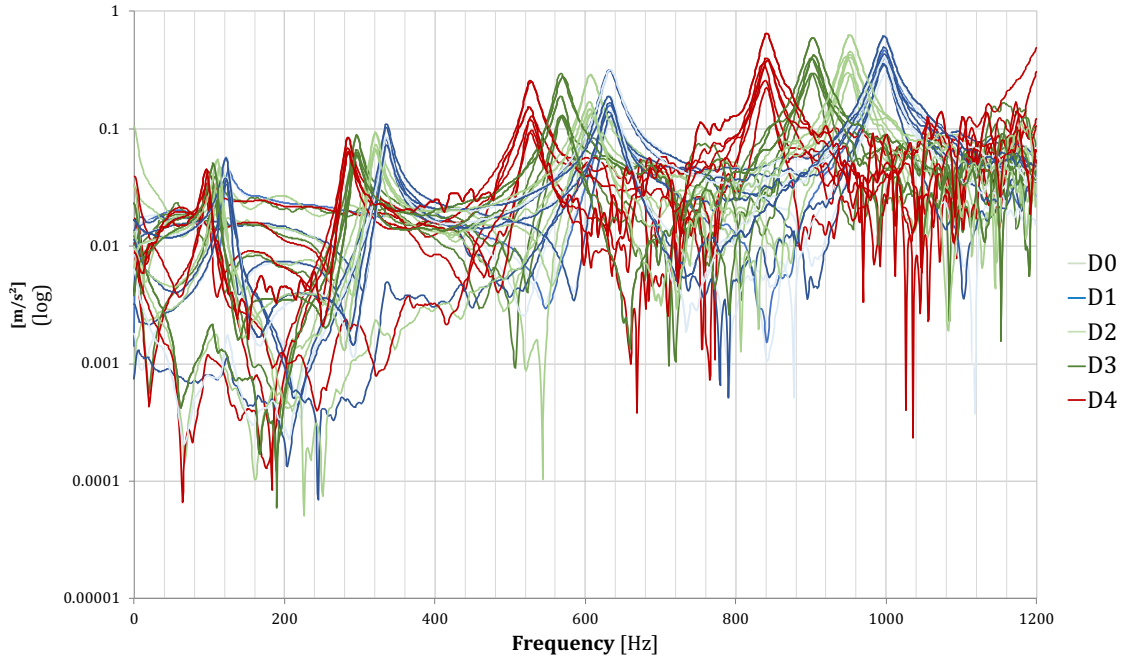

Figure 32 – Envelope of FRFs for strengthened beam B2 with free-free ends at different damage degrees *Di*=0, 1…, 4 by static bending tests.

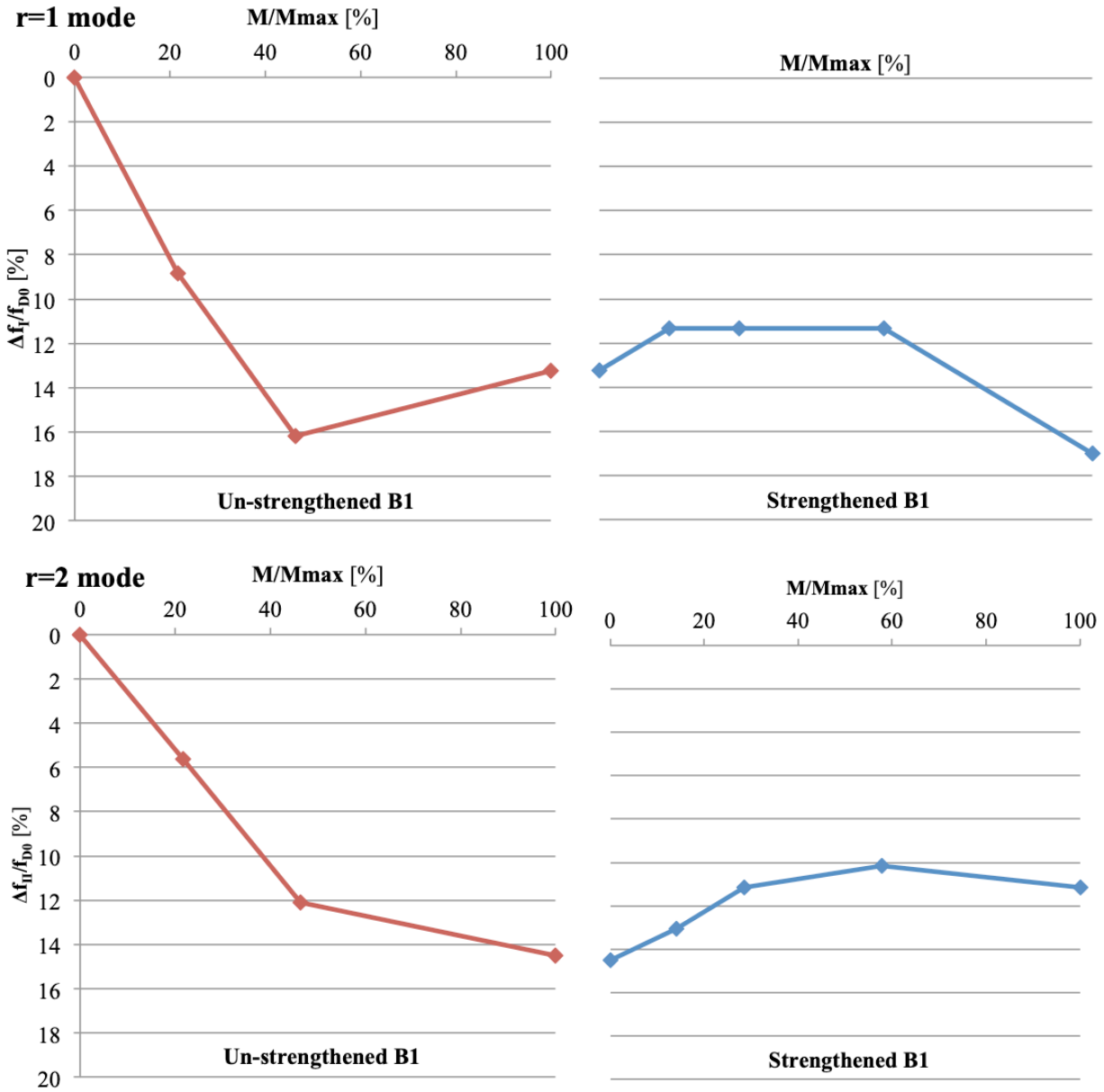
r=1 mode
M/Mmax [%]
0
20
40
60
80
100
0
2
4
6
8
10
12
14
16
18
20
$\Delta f_I/f_{D0}$ [%]
Un-strengthened B1
M/Mmax [%]
Strengthened B1
r=2 mode
M/Mmax [%]
0
20
40
60
80
100
0
2
4
6
8
10
12
14
16
18
20
$\Delta f_{II}/f_{D0}$ [%]
Un-strengthened B1
M/Mmax [%]
0
20
40
60
80
100
Strengthened B1

(a)

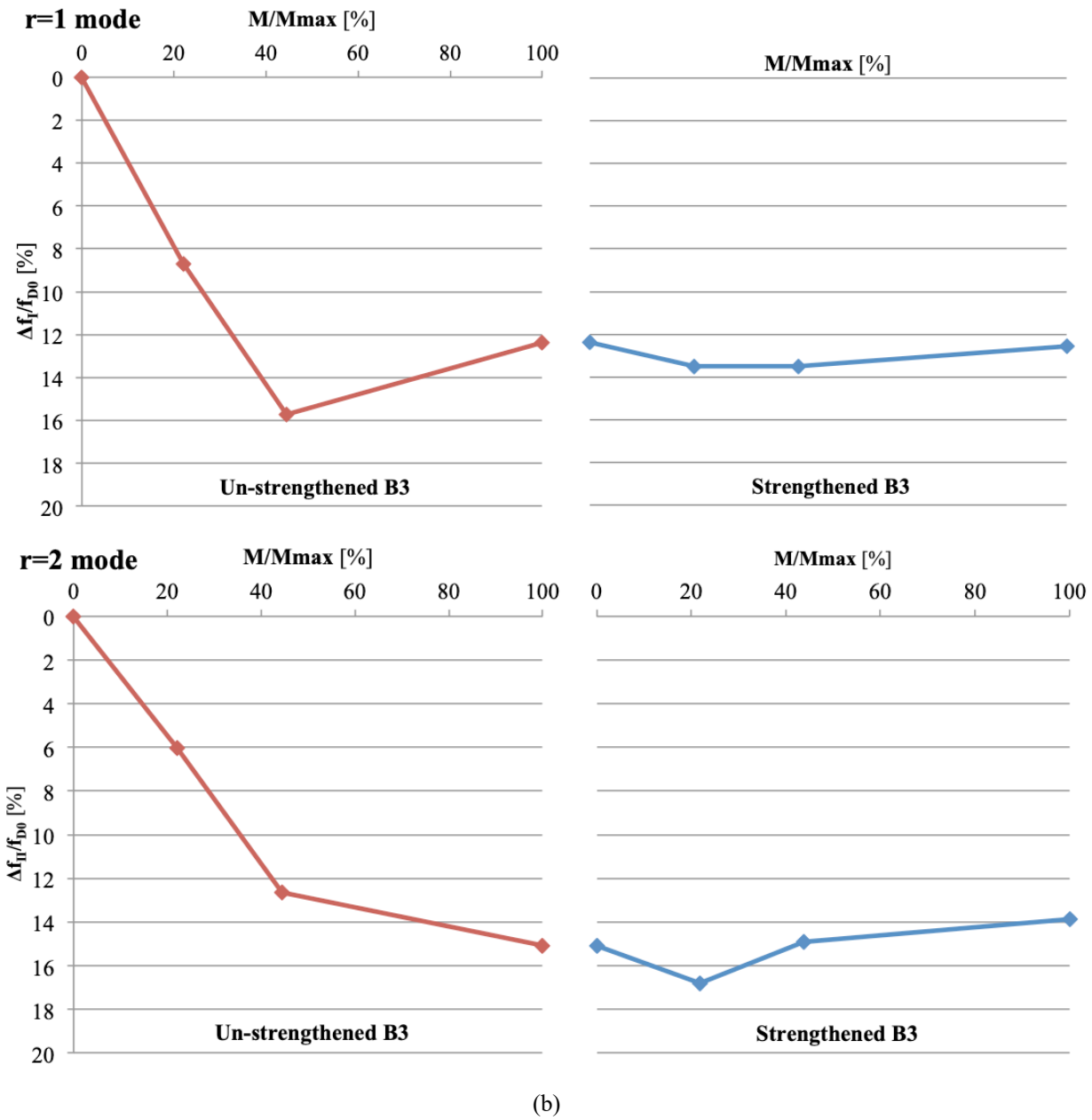

(b)

Figure 33 –Exp. diagrams of variation of frequency values (%) for the first two modes r = 1,2 vs moment ratio M/M_{max} (%) for beams (a) B1 and (b) B3.

List of Tables:

Table 1 – Geometric and mechanical characteristic of GFRP rod.

GFRP Circular rod	Diameter d_{GFRP} [mm]	Section area A_{GFRP} [mm^2]	Exp. tensile strength f_{GFRP} [N/mm^2]	Exp. Young's modulus E_{GFRP} [kN/mm^2]
	9.52	71.26	1040	33.6

Table 2 – Exp. results for beam B1 by static bending test at damage degree *Di*.

Damage steps	Load [kN]	Deflection at midspan [mm]	Strain at compressive concrete ε_c (‰)	Strain at steel reinforcement (intrados) ε_s (‰)	Curvature of midspan section χ (10^{-5})
D1	4.00	1.40	0.23	0.67	0.67
D2	8.00	4.56	0.46	1.45	1.47
D3	18.00	10.78	0.99	3.35	3.30

Table 3 – Exp. results for strengthened beam B1 by static bending test at damage degree *Di*.

Damage steps	Load [kN]	Deflection at midspan [mm]	Strain at compressive concrete ε_c (‰)	Strain at steel reinforcement (intrados) ε_s (‰)	Strain at GFRP rod ε_{GFRP} (‰)	Curvature of midspan section* χ (10^{-5})
D1	4.0	1.63	0.17	0.46	0.29	0.31
D2	8.0	3.75	0.38	1.04	0.66	0.695
D3	16.0	7.54	0.77	2.13	1.47	1.50
D4	28.0	17.50	1.98	5.61	6.04	5.30

*Curvature with strain on compressive edge and GFRP rod.

Table 4 – Exp. results for strengthened beam B2 by static bending test at damage degree *Di*.

Damage steps	Load [kN]	Deflection at midspan [mm]	Strain at compressive concrete ε_c (‰)	Strain at steel reinforcement (intrados) ε_s (‰)	Strain at epoxy resin ε_{res} (‰)	Curvature of midspan section* χ (10^{-5})
D1	4.0	0.61	0.095	0.084	0.34	0.41
D2	8.0	2.83	0.36	1.12	1.14	1.74
D3	16.0	8.80	0.82	2.51	2.89	4.15
D4	28.0	20.96	1.56	7.37	6.81	10.91

*Curvature with strain on compressive edge (resin) and steel bar.

Table 5 – Exp. results for beam B3 by static bending test at damage degree *Di*.

Damage steps	Load [kN]	Deflection at midspan [mm]	Strain at compressive concrete ε_c (‰)	Strain at steel reinforcement (intrados) ε_s (‰)	Curvature of midspan section χ (10^{-5})
D1	4.0	2.30	0.22	0.39	0.48
D2	8.0	5.45	0.45	1.62	1.59
D3	18.0	12.59	0.88	3.27	3.19

Table 6 – Exp. results for strengthened beam B3 by static bending test at damage degree *Di*.

Damage steps	Load [kN]	Deflection at midspan [mm]	Strain at compressive concrete ε_c (‰)	Strain at steel reinforcement (intrados) ε_s (‰)	Strain at GFRP rod ε_{GFRP} (‰)	Curvature of midspan section* χ (10^{-5})
D1	4.0	1.90	0.24	0.48	0.37	0.56
D2	8.0	4.39	0.53	1.14	0.83	1.36
D3	18.0	10.23	1.11	2.56	1.23	3.02

*Curvature with strain on compressive edge and steel bar.

Table 7 – Geometric and mechanical parameters of RC beams under vibration.

Width b [mm]	Thickness t [mm]	Length L [mm]	Young's modulus E_c [kN/mm^2]	Density ρ [Ns^2 /mm^4]	Moment of inertia I [mm^4]
120	160	2200	34.50	$2.43 \cdot 10^{-9}$	$3.89 \cdot 10^{7}$

Table 8 – Frequency values for undamaged beam models in different end conditions.

Boundary conditions	f_1 (Hz)	f_2 (Hz)	f_3 (Hz)	f_4 (Hz)
Theor. EB uniform beam free-free ends	126.20	347.70	681.80	1126.48
Theor. EB uniform beam hinge-hinge ends	64.18	222.51	500.66	890
Exp. average values free-free ends – beam B1	130	350	659	1035
Exp. average values hinge-hinge ends – beam B1	68	248	679	1095
Exp. average values free-free ends –beam B3	129.46	343.57	645.49	1118.30
Exp. average values hinge-hinge ends – beam B3	67.63	249.32	645.15	1046.89

Table 9 – Exp. average frequency values at damage degree *Di* for un-strengthened beam B1 (hinge-hinge end condition).

Damage degree	f_1 (Hz)	$\Delta f_1/f_{D0}$ (%)	f_2 (Hz)	$\Delta f_2/f_{D0}$ (%)	f_3 (Hz)	$\Delta f_3/f_{D0}$ (%)	f_4 (Hz)	$\Delta f_4/f_{D0}$ (%)
D0	68	-	248	-	679	-	1095	-
D1	62	8.82	234.00	5.65	624.00	8.10	1045.00	4.57
D2	57	16.18	218.00	12.10	599.00	11.78	965.00	11.87
D3	59	13.24	212.00	14.52	595.00	12.37	948.00	13.42

Table 10 – Exp. average frequency values at damage degree *Di* for strengthened beam B1 (hinge-hinge end condition).

Damage degree	f_1 (Hz)	$\Delta f_1/f_{D0}$ (%)	f_2 (Hz)	$\Delta f_2/f_{D0}$ (%)	f_3 (Hz)	$\Delta f_3/f_{D0}$ (%)	f_4 (Hz)	$\Delta f_4/f_{D0}$ (%)
D0(*)	53	-	207	-	552	-	865	-
D1	54	-1.89	210	-1.45	565	-2.36	875	-1.16
D2	54	-1.89	214	-3.38	560	-1.45	877	-1.39
D3	54	-1.89	216	-4.35	561	-1.63	887	-2.54
D4	51	3.77	214	-3.38	548	0.72	850	1.73

(*) Undamaged condition is at the beginning of vibration test for strengthened beam.

Table 11 – Exp. average frequency values at damage degree *Di* for un-strengthened beam B3 (free-free end condition).

Damage degree	f_1 (Hz)	$\Delta f_1/f_{D0}$ (%)	f_2 (Hz)	$\Delta f_2/f_{D0}$ (%)	f_3 (Hz)	$\Delta f_3/f_{D0}$ (%)	f_4 (Hz)	$\Delta f_4/f_{D0}$ (%)
D0	129.46	-	343.57	-	645.49	-	1118.30	-
D1	94.90	26.70	306.96	10.66	559.51	13.32	871.76	22.05
D2	84.23	34.94	250.93	26.96	488.20	24.37	811.66	27.42
D3	95.94	25.89	257.64	25.01	479.82	25.67	804.79	28.03

Table 12 – Exp. average frequency values at damage degree *Di* for strengthened beam B3 (free-free end condition).

Damage degree	f_1 (Hz)	$\Delta f_1/f_{D0}$ (%)	f_2 (Hz)	$\Delta f_2/f_{D0}$ (%)	f_3 (Hz)	$\Delta f_3/f_{D0}$ (%)	f_4 (Hz)	$\Delta f_4/f_{D0}$ (%)
D0 (*)	102.95	-	275.84	-	520.17	-	852.29	-
D1	96.35	6.41	265.25	3.84	502.64	3.37	809.60	5.01
D2	95.14	7.59	261.02	5.37	493.88	5.05	790.80	7.21
D3	94.49	8.22	258.23	6.38	489.14	5.97	785.08	7.89

(*) Undamaged condition is at the beginning of vibration test for strengthened beam

Table 13 – Exp. average frequency values at damage degree *Di* for un-strengthened beam B3 (hinge-hinge end condition).

Damage degree	f_1 (Hz)	$\Delta f_1/f_{D0}$ (%)	f_2 (Hz)	$\Delta f_2/f_{D0}$ (%)	f_3 (Hz)	$\Delta f_3/f_{D0}$ (%)	f_4 (Hz)	$\Delta f_4/f_{D0}$ (%)
D0	67.63	-	249.32	-	645.15	-	1046.89	-
D1	61.75	8.69	234.25	6.05	625.50	3.05	1044.50	0.23
D2	57.00	15.72	217.75	12.66	599.75	7.04	967.75	7.56
D3	59.25	12.39	211.75	15.07	596.00	7.62	948.00	9.45

Table 14 – Exp. average frequency values at damage degree *Di* for strengthened beam B3 (hinge-hinge end condition).

Damage degree	f_1 (Hz)	$\Delta f_1/f_{D0}$ (%)	f_2 (Hz)	$\Delta f_2/f_{D0}$ (%)	f_3 (Hz)	$\Delta f_3/f_{D0}$ (%)	f_4 (Hz)	$\Delta f_4/f_{D0}$ (%)
D0 (*)	54.35	-	213.69	-	542.03	-	845.56	-
D1	53.75	1.10	210.00	1.73	564.86	-4.21	875.00	-3.48
D2	53.75	1.10	214.00	-0.14	560.00	-3.32	876.50	-3.66
D3	54.25	0.18	216.25	-1.20	560.57	-3.42	887.00	-4.90

(*) Undamaged condition is at the beginning of vibration test for strengthened beam.

Table 15 – Exp. average frequency values at damage degree *Di** by notches for strengthened beam B2 (free-free end condition).

Damage degree	f_1 (Hz)	$\Delta f_1/f_{D0}$ (%)	f_2 (Hz)	$\Delta f_2/f_{D0}$ (%)	f_3 (Hz)	$\Delta f_3/f_{D0}$ (%)	f_4 (Hz)	$\Delta f_4/f_{D0}$ (%)
D0* - No nothches	128	-	342	-	640	-	1014	-
D1* - 1 notch	128	0.00	342	0.00	634	0.94	1016	-0.20
D2* - 3 notches	124	3.13	338	1.17	626	2.19	998	1.58
D3* - 5 notches	120.67	5.73	334	2.34	627	2.03	986	2.76

Table 16 – Exp. average frequency values at damage degree *Di* by static bending test for strengthened beam B2 (free-free end condition).

Damage degree	f_1 (Hz)	$\Delta f_1/f_{D0}$ (%)	f_2 (Hz)	$\Delta f_2/f_{D0}$ (%)	f_3 (Hz)	$\Delta f_3/f_{D0}$ (%)	f_4 (Hz)	$\Delta f_4/f_{D0}$ (%)
D0	121.00	-	333.14	-	631.25	-	997.75	-
D1	121.17	-0.14	333.67	-0.16	629.25	0.32	996.75	0.10
D2	112.00	7.44	319.33	4.15	604.88	4.18	949.75	4.81
D3	106.33	12.12	292.33	12.25	566.25	10.30	899.63	9.83
D4	93.50	22.73	280.50	15.80	524.25	16.95	837.63	16.05

Table 17 – Values of lag coefficient k for strengthened beams B1 and B3.

	Damage steps	Load P [kN]	k_1	$k_{1,av}$	k_2	$k_{2,av}$
B1	**D1**	4.00	0.63	0.65	0.48	0.46
	D2	8.00	0.64		0.47	
	D3	16.00	0.69		0.43	
B3	**D1**	4.00	0.77	0.66	0.37	0.46
	D2	8.00	0.73		0.41	
	D3	18.00	0.48		0.61	